

Von Kármán vortex street

author:

Yas Tahmaseb Zadeh Ahrabi 400105874

Course:

Fluid Mechanics II

Professor:

Dr. Karimi

Fall Semester 1402-1403

Contents

1	Abs	stract	1					
2	Intr	roduction	2					
3	Steady, Laminar vortex shedding							
	3.1	Low Reynolds regime, Circular section	3					
	3.2	3.1.1 Geometrical Settings3.1.2 Appropriate Meshing3.1.3 Simulation3.1.4 ConclusionLow Reynolds regime, Elliptical section	3 4 5 6 10					
	3.3	3.2.2 Appropriate Meshing	10 10 12 13 17					
		3.3.2 Appropriate Meshing	17 17 17 18					
4	Tra	nsient, Laminar vortex shedding	22					
	4.1	Moderate Reynolds regime, Elliptical section	22					
	4.2	4.1.4 Conclusion	22 22					
		4.2.2 Appropriate Meshing	30 30 30 31					
5	Stea	ady, Turbulent vortex shedding	3 6					
	5.1	High Reynolds regime. Elliptical section	36					

		5.1.1 5.1.2 5.1.3 5.1.4	Appropriate Meshing	36 36 37 38			
6	Concluding remarks						
7	Appendix						
	7.1	Article	S	j			
		7.1.1 7.1.2	Fluid Flow Around and Heat Transfer from Elliptical Cylinders, 2005 Steady flow of power-law fluids across an unconfined elliptical cylinder, 2006	j			
	7.2	7.1.3 7.1.4 Books	Summary of drag coefficients of various shaped cylinders, 1957 Vortex dynamics in the wake, 1996	j j			
	7.3	7.2.1 Additio	Fundamentals of Fluid Mechanics, Edition six	j			
	7.4	7.3.1 7.3.2 7.3.3 7.3.4 7.3.5 7.3.6 7.3.7 Anima	Vorticity diffusion and boundary layer	ii iii iii iii iii			
		7.4.1 7.4.2	Velocity animation for the Transient, Laminar regime in Moderate Reynolds Velocity animation for the Transient, Laminar regime in High Reynolds .	ii ii			

1. Abstract

Flow past cylindrical bodies has always been and forever will be an important classical problem in Fluid Mechanic and Heat Transfer studies, as its results can be very determinant and of help in the computation of diverse shapes and configurations against arbitrary flows.

Although flow past cylindrical bodies itself has a simple configuration, yet it provides a great and comprehensive insight into many physical phenomena regarding flow past thick bodies, such as separation, formation of separation, vortex shedding and etc.

Studies demonstrate that flow past thick bodies alter pertaining to the configurations and conditions applied. Considering a laminar, low Reynolds flow, no separation or vortex shedding is expected, yet as it follows within higher Reynolds, attached and symmetrical wakes start to appear. When the Reynolds number reaches it's critical value, the flow becomes unsteady as it transitions from laminar to turbulent, causing harmonic and two-dimensional vortex separations throughout the flow, and as the Reynolds number gains higher values, the turbulence effects get even more explicit.

The Von Kármán vortex street, a repeating pattern of swirling vortices, caused by vortex shedding which is responsible for the unsteady separation of flow, is a phenomenon of great importance to us.

Flow past bodies becomes separated from the surface at times due to the positive pressure gradient created behind the body, this adverse pressure gradient creates a wake region which in time causes the oscillatory Von Kármán vortex street phenomenon.

Such phenomena can be observed ed within various scales, from flow across an instrumental string to flow across large islands as demonstrated in figure 1.1.



Figure 1.1: Kármán vortex street caused by wind flowing around the Juan Fernández Islands off the Chilean coast

2. Introduction

In this project, we are aiming to simulate incompressible, Newtonian fluid flow across cylindrical sections and study the flow characteristics in diverse configurations such as laminar or turbulent flow in steady or transient states to help us furthermore understand the topics discussed in this course.

Technically the flow over any body considered two-dimensional is a flow over a cylindrical body, the flow characteristics along the cylinder's axis might vary considerably as the Reynolds number gains high values, yet in this project we consider the bodies two dimensional and neglect the changes along the cylinder's axis intentionally to reduce the computation cost.

the project consists of six individual parts demonstrated in the table below. For each config-

project	Regime	Geometry	Reynolds
1	Steady, Laminar	Circle	2
2	Steady, Laminar	Ellipse	5
3	Steady, Laminar	Ellipse	20
4	Transient, Laminar	Ellipse	300
5	Transient, Laminar	Ellipse	900
6	Steady, Turbulent	Ellipse	100000

Table 2.1: Configurations for each part of the project

*The circle's diameter is considered 1 m and the ellipse's aspect ratio is 1.7, with smaller diameter as 1 m, denoting the diameter perpendicular to the flow

uration if the flow velocity is expressed by U, and outlet pressure is considered the pressure on the upper, lower and right side of the two-dimensional cylinder whilst the inlet pressure is the pressure on it's left side (considering glow from left to right), the Reylonds and Strouhal numbers are defined as below.

$$Re = \frac{DU}{\nu} \tag{2.1}$$

$$Re = \frac{DU}{\nu}$$

$$St = \frac{fD}{U}$$
(2.1)

If the geometry in question is circular, parameter D is related to it's diameter and if it's elliptical the parameter is referring to it's diameter perpendicular to flow. Parameter f is denoting the vortices frequencies and ν denoting kinematic viscosity.

3. Steady, Laminar vortex shedding

For the first three configurations discussed in this part, a steady, laminar flow is studied, given various geometry and Reynolds regimes. With the help of fluid simulation software, ANSYS Fluent, each configuration is met with its own particular geometrical settings specifying the domain sufficient for computation, furthermore followed by its appropriate meshing style taking into account the flow regime. Afterwards it's setup for computation to yield the desired parameters and be analogized with the related articles presented in chapter 7.

3.1 Low Reynolds regime, Circular section

3.1.1 Geometrical Settings

Using SpaceClaim to design the specific geometry, as we are met with a circular configuration demonstrated in Table 2.1, row 1, a circular geometry is utilized. Before sketching, the units for the configuration is set in meters and afterwards the surfaces are sketched in the xy plane. Circular cylinder itself is of 1 m diameter and the surrounding area is estimated to be of a 15 m radius, as demonstrated in figure 3.1.

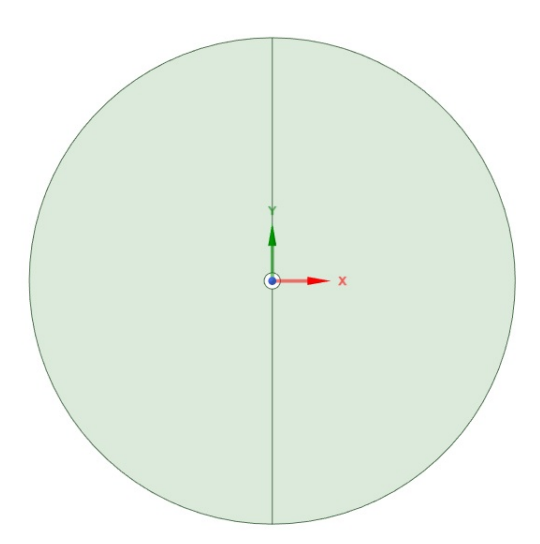


Figure 3.1: Geometry assigned in SpaceClaim for the Low Reynolds, Steady, Laminar simulation of flow against circular cylinder

The surrounding area has been split in two, making it able to distinguish the inlet area from the outlet area.

3.1.2 Appropriate Meshing

Facing a simple circular geometry, a simple MultiZone Quad/Tri meshing with All Quad free face mesh method, has been implemented purposefully considering quad meshes (structured meshes) provide higher quality solutions with fewer nodes with an overall statistics of 2176 nodes. Alongside quad meshing, Edge Sizing for the two split lines with a growing bias type from the cylinders surface to the surrounding surface, having a bias factor, 35, and a number of divisions, 30, has been used. The global meshing element size is set as 1.5 m. Furthermore changes in the meshing would be applied later to study mesh convergence. A schematic of the meshing is given in figure 3.2.

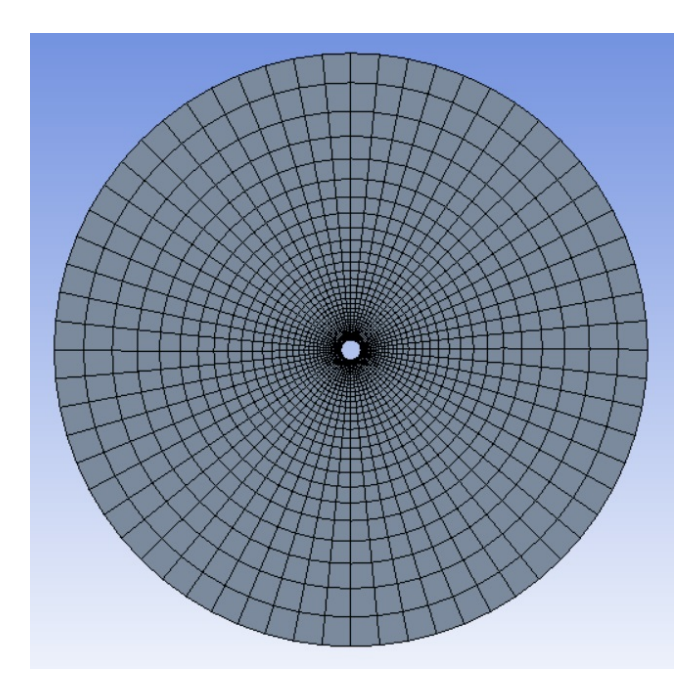


Figure 3.2: Appropriate meshing for the Low Reynolds, Steady, Laminar simulation of flow against circular cylinder

Of course the inlet, outlet, wall and fluid sections would be named using named selections option for each edge or surface, so that the simulation would go smoothly without problems. As we have a Structured meshing the Element Quality is also very high!

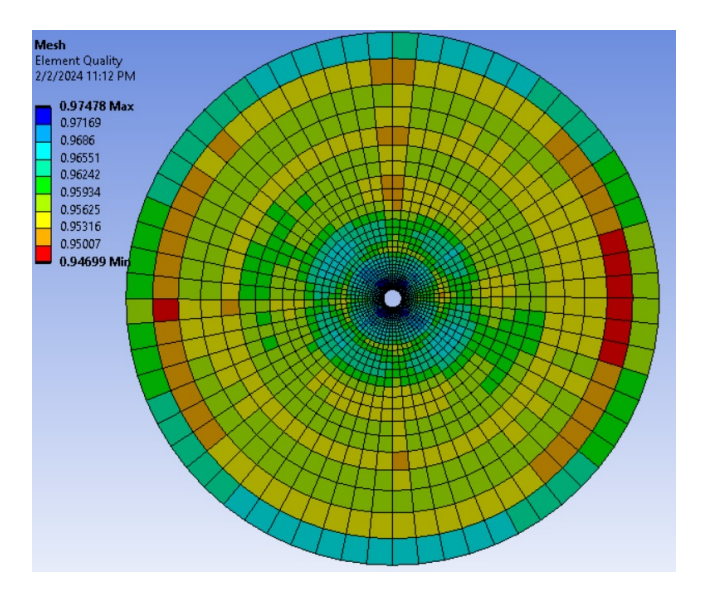


Figure 3.3: Mesh Element Quality for the Low Reynolds, Steady, Laminar simulation of flow against circular cylinder

3.1.3 Simulation

As the simulation is approached having specified the proper geometry and meshing, for computation, the option double precision is checked before launching the simulation and also 4 solver processes are used in order to get the desired results.

The modified settings for the configuration given in Table 2.1; Pressure Based, Steady solver, Viscous(laminar) in Models, air as specific fluid in Cell Zone Conditions, inlet velocity set $3(10^{-5}) \frac{m}{s}$ regarding the given Reynolds, 2, measured by equation 2.1 and Velocity Specification Method, Magnitude and Direction, and finally setting the Reference value as the inlet velocity, is applied.

Afterwards the solution method is set as coupled with the gradient settings set as the Least Squares Cell Based option considering it's the one choice with the optimal computational cost, and furthermore setting the Pressure's equation interpolation as second order and the Momentum's equation as second order upwind.

Following up we set up two report definitions for the Drag and Lift Coefficients, using the right force vectors, perpendicular to stream for lift and parallel to stream for drag, making sure the wall zone is well selected.

As it is desired to have the meshing converge we take the Check Convergence options in Residual Monitors off and set enough iterations to reach convergence ourselves.

Eventually using Hybrid Initialization, recommended for steady flows the initialization is done and using 200 iterations the simulation can be done.

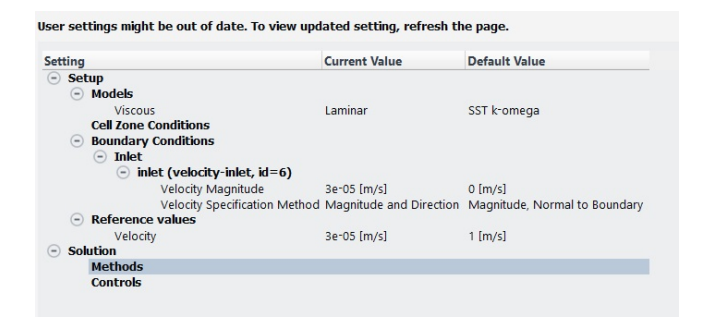


Figure 3.4: Summary of setting up options for the Low Reynolds, Steady, Laminar simulation of flow against circular cylinder

Computation with such settings yields the Drag and Lift Coefficients charts demonstrated in figure 3.11 and 3.12 further in the text, yet here for verifying mesh convergence, the setup used for meshing in part 3.1.2, changes respectively upgrading the nodes, approximately computing the Drag coefficient with new node statistics 1.5 times the previous nodes each time. For this matter the Element size is made less each time and the Number of Divisions or Bias Factor for Edge Sizing is also increased, each multiplied or divide by $\sqrt{1.5}$!

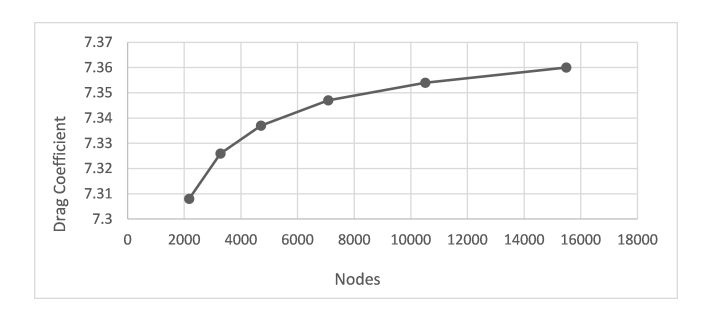


Figure 3.5: Mesh Convergence for the Low Reynolds, Steady, Laminar simulation of flow against circular cylinder

As figure 3.5 demonstrates, convergence is happening and small changes are occurring while the amount of nodes is becoming of higher value, therefore there's only extra computational cost without much difference and the optimal meshing is the one explained aforementioned.

3.1.4 Conclusion

Using the setup explained in section 3.1.3, Velocity, Pressure and Vorticity Contours and the Stream line Pathlines can be obtained. As the computation is done, the Graphics section is ready for use. In the Contours section using Velocity contours, Velocity Magnitude and Vorticity Magnitude, and Pressure contour, Static pressure, figures 3.6 to 3.8 are derived. Furthermore using Pathlines for Velocity, Stream Function with 10 path skips and 500 steps, the Streamline Graphics are also yielded, demonstrated in figure 3.9.

^{*}Any other options needed is set as the software's default

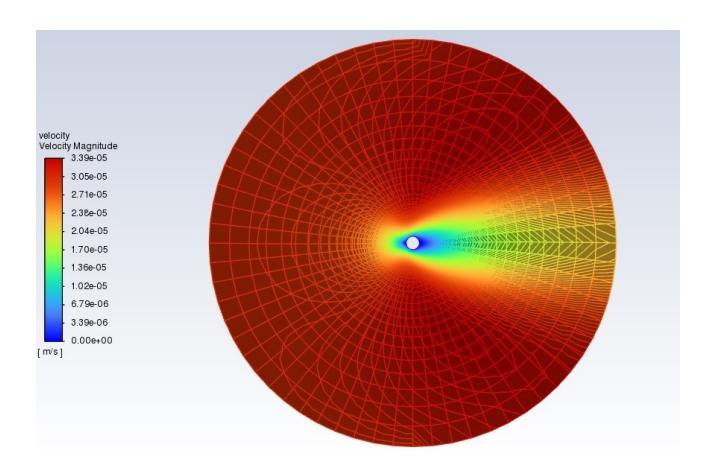


Figure 3.6: Velocity Contour for the Low Reynolds, Steady, Laminar simulation of flow against circular cylinder

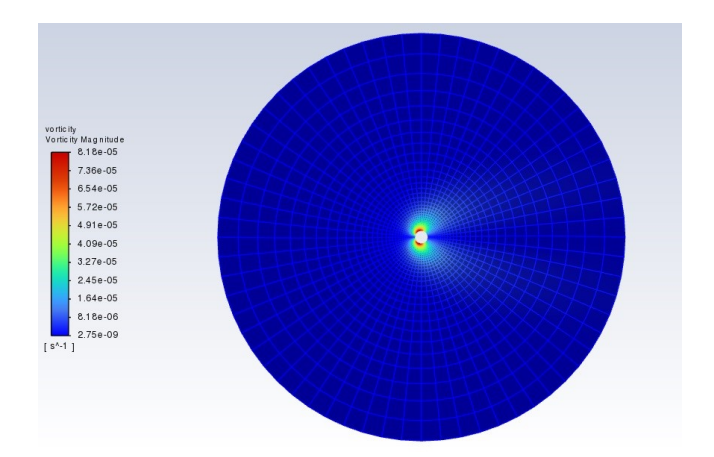


Figure 3.7: Vorticity Contour for the Low Reynolds, Steady, Laminar simulation of flow against circular cylinder

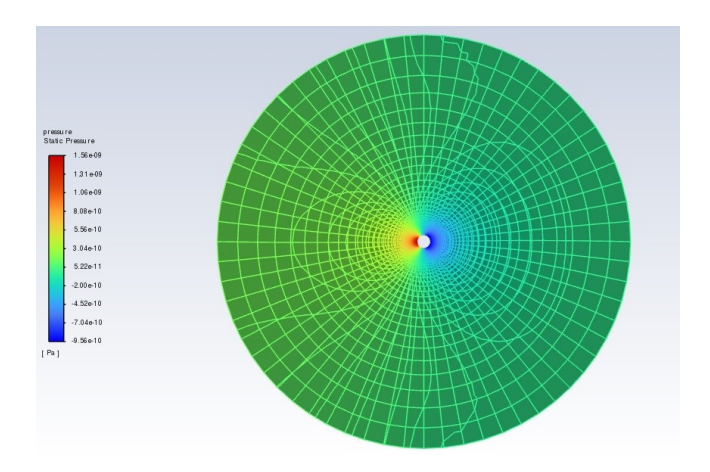


Figure 3.8: Pressure Contour for the Low Reynolds, Steady, Laminar simulation of flow against circular cylinder

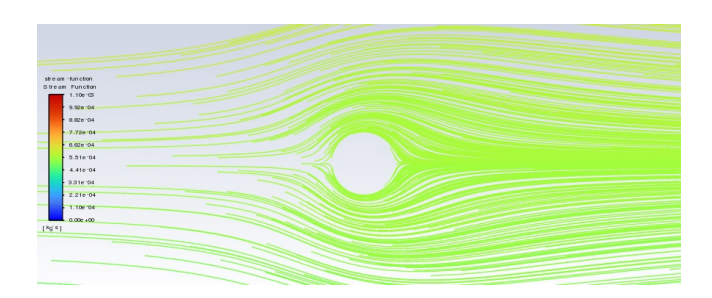


Figure 3.9: Streamline Graphics for the Low Reynolds, Steady, Laminar simulation of flow against circular cylinder

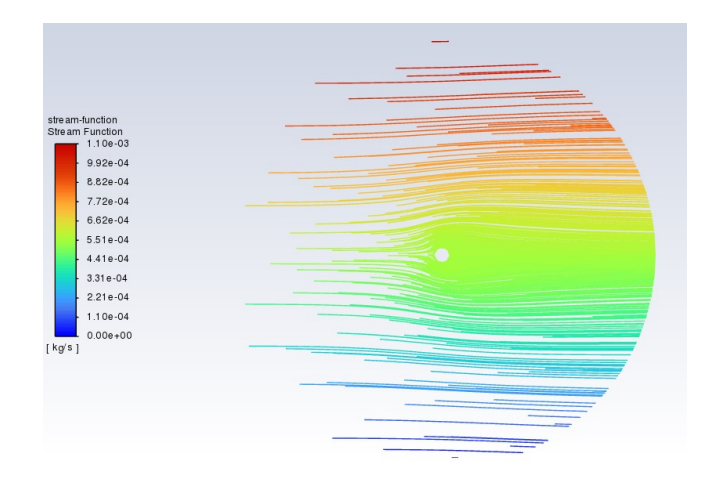


Figure 3.10: Streamline Graphics for the Low Reynolds, Steady, Laminar simulation of flow against circular cylinder

As expected for this regime with such low Reynolds, no separation has occurred and the flow has smoothly passed the cylinder with no wake regions as demonstrated in figure 3.9 and 3.10. In figure 3.10 it is also obvious that streamlines are not effected by the cylinder far from it and they are pretty straight as the original flow!

Like what was predicted also, the Velocity decreases around the cylindrical surface and there is a separation point infront and behind the cylinder at 0 and 180 degrees, as demonstrated in figure 3.6. It is also clear from figure 3.7 that in these previously mentioned points the pressure respectively reaches it's maximum and minimum values. At the end there are small vortices created due to the boundary layer conditions on the cylinder that are inconsiderable and are stronger closer to the cylinder over the inlet section as shown in figure 3.8. The growth of boundary layers is related to vorticity transport and for ow over the body, vorticity generated at the leading edge is advected by the ow, while diusing away from the body. furthermore explanation of this is given in appendix 7.3.1 and 7.3.2 by two articles.

The Lift Coefficient computed in this simulation, 0.0002 is inconsiderable whilst there is such larger Drag Coefficient computed, 7.308. In this low Reynolds regime, the Drag Coefficient is mostly Frictional and has somewhat of a linear connection with the Reynolds number on a logarithmic scale! A great way to check the simulation is by using Figure 9.21(a) in the book shared in appendix 7.2, for the cylindrical surface it is very close. Checking this computation with the article given in appendix 7.1.1, there is some inconsiderable difference with the theoretical value yielded by the equation below (equation 45 of the article).

$$C_D = \frac{5.786}{\sqrt{Re_{l_D}}} + 1.152 + \frac{1.260}{Re_{l_D}} = 5.873 \implies 24\% variance$$

The Report Definition charts for Lift and Drag Coefficients are demonstrated in figures 3.11 and 3.12.

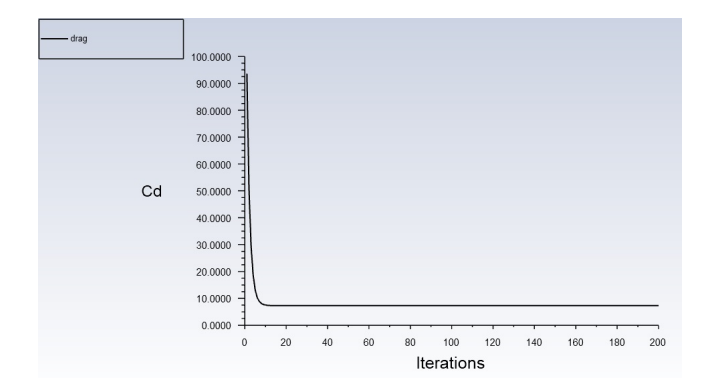


Figure 3.11: Drag Coefficient chart for the Low Reynolds, Steady, Laminar simulation of flow against circular cylinder

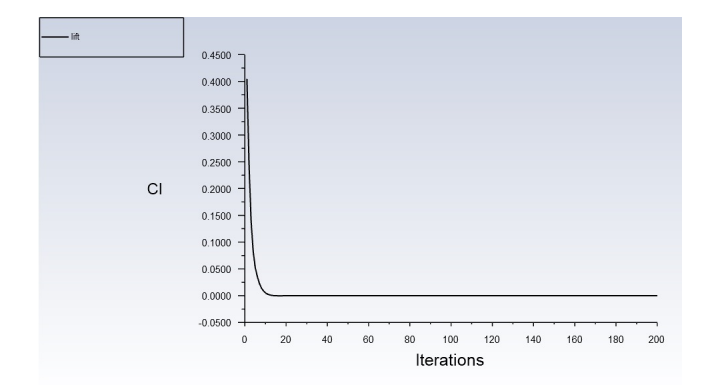


Figure 3.12: Lift Coefficient chart for the Low Reynolds, Steady, Laminar simulation of flow against circular cylinder

3.2 Low Reynolds regime, Elliptical section

3.2.1 Geometrical Settings

Using SpaceClaim to design the specific geometry, as we are met with an elliptical configuration demonstrated in Table 2.1, row 2, an elliptical geometry is utilized. Before sketching, the units for the configuration is set in meters and afterwards the surfaces are sketched in the xy plane. Elliptical cylinder itself is of 1 m diameter perpendicular to flow and 1.7 m parallel to it and the surrounding area is estimated to be formed by two circular parts, one of a 5 m radius around the elliptical surface and one two-dimensional cylindrical shell surrounding that with an inner radius of 5 m and outer diameter of 45 m, as demonstrated in figure 3.13.

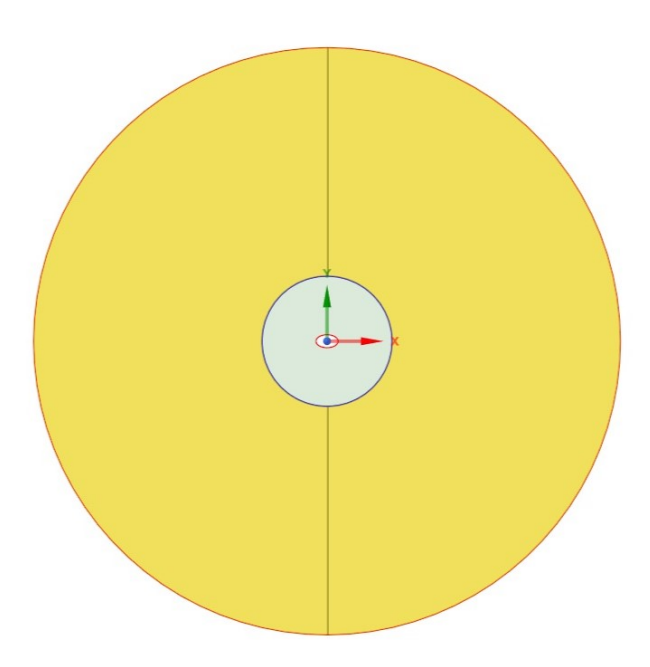


Figure 3.13: Geometry assigned in SpaceClaim for the Low Reynolds, Steady, Laminar simulation of flow against elliptical cylinder

The surrounding area has been split in two, making it able to distinguish the inlet area from the outlet area.

3.2.2 Appropriate Meshing

Facing an elliptical geometry there has to be a more complex meshing than what was done for circular cylinder in 3.1.2. An optimal proposed meshing is to use inflation with 10 layers of 1.2 growth rate alongside an Edge Sizing for the wall with a Number of Divisions, 750, to get the perfect boundary layer layout. Afterwise All Triangles method for the inner circular area around the ellipse and at last Structured Face Meshing using Quadrilaterals and alongside quad meshing, Edge Sizing for the two split lines with a growing bias type from the cylinders surface of the inner circular area to the surrounding surface, having a bias factor, 6, and a number of divisions, 70, has been used. The global meshing element size is set at 0.2 m. Furthermore changes in the meshing would be applied later to study mesh convergence. A schematic of the meshing is given in figure 3.14.

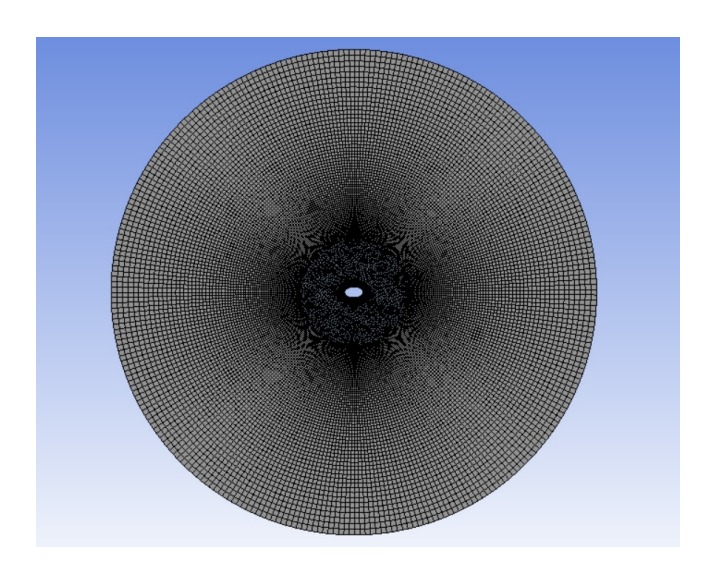


Figure 3.14: Appropriate meshing for the Low Reynolds, Steady, Laminar simulation of flow against elliptical cylinder

Of course the inlet, outlet, wall and fluid sections would be named using named selections option for each edge or surface, so that the simulation would go smoothly without problems. As the meshing is not fully Structured the Element Quality in such areas where the meshing method is All Triangles is lower than the structured surrounding and boundary layer meshing.

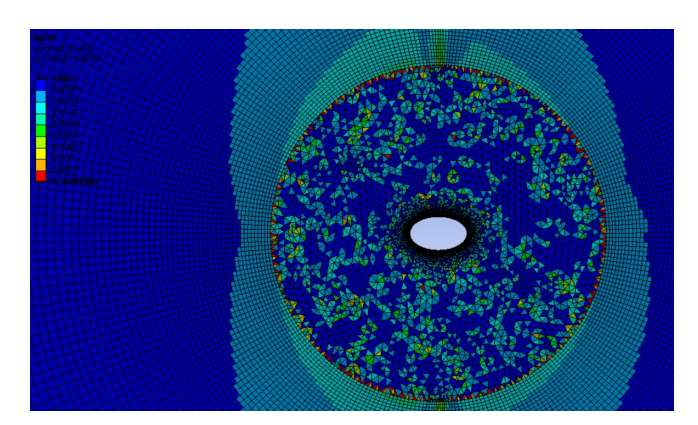


Figure 3.15: Mesh Element Quality for the Low Reynolds, Steady, Laminar simulation of flow against elliptical cylinder

Another option for meshing is to use O-type meshing around the ellipse, in this case with a surrounding area of diameter 45 m, and four splitting edges two perpendicular to flow and two parallel, global element size set to 0.3 m and Edge Sizing for wall edge, Number of Divisions 80, Edge Sizing for the four splits, Number of Divisions, 160, with a Bias Factor of 28, yields 51520 nodes and after computation a Drag Coefficient very close to the one executed by the original mesh introduced, is executed! Therefore since it has considerably more nodes (nearly twice) and as it follows higher computational cost, the original mesh is the optimal meshing, Although for this O-type mesh the Element quality is higher than the previous one considering it's more structured!

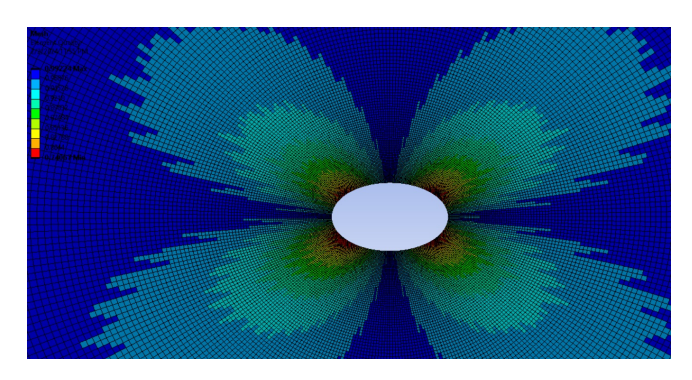


Figure 3.16: Mesh Element Quality (O-type) for the Low Reynolds, Steady, Laminar simulation of flow against elliptical cylinder

3.2.3 Simulation

As the simulation is approached having specified the proper geometry and meshing, for computation, the option double precision is checked before launching the simulation and also 4 solver processes are used in order to get the desired results.

The modified settings for the configuration given in Table 2.1; Pressure Based, Steady solver, Viscous(laminar) in Models, air as specific fluid in Cell Zone Conditions, inlet velocity set $7.5(10^{-5}) \frac{m}{s}$ regarding the given Reynolds, 5, measured by equation 2.1 and Velocity Specification Method, Magnitude and Direction, and finally setting the Reference value as the inlet velocity, is applied.

Afterwards the solution method is set as coupled with the gradient settings set as the Least Squares Cell Based option considering it's the one choice with the optimal computational cost, and furthermore setting the Pressure's equation interpolation as second order and the Momentum's equation as second order upwind.

Following up we set up two report definitions for the Drag and Lift Coefficients, using the right force vectors, perpendicular to stream for lift and parallel to stream for drag, making sure the wall zone is well selected.

As it is desired to have the meshing converge we take the Check Convergence options in Residual Monitors off and set enough iterations to reach convergence ourselves.

Eventually using Hybrid Initialization, recommended for steady flows the initialization is done and using 300 iterations the simulation can be done.

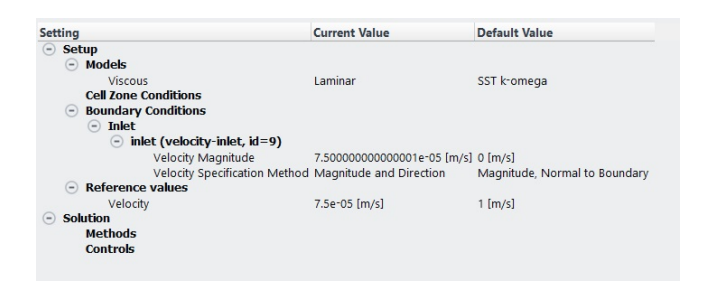


Figure 3.17: Summary of setting up options for the Low Reynolds, Steady, Laminar simulation of flow against elliptical cylinder

Computation with such settings yields the Drag and Lift Coefficients charts demonstrated in figure 3.24 and 3.25 further in the text, yet here for verifying mesh convergence, the setup used for meshing in part 3.2.2, changes respectively upgrading the nodes, approximately computing the Drag coefficient with new node statistics 1.5 times the previous nodes each time.

^{*}Any other options needed is set as the software's default

For this matter the Element size is made less each time and the Number of Divisions or Bias Factor for Edge Sizing is also increased, each multiplied or divide by $\sqrt{1.5}$!

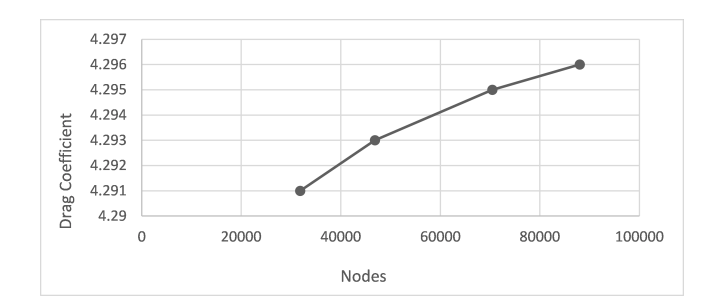


Figure 3.18: Mesh Convergence for the Low Reynolds, Steady, Laminar simulation of flow against elliptical cylinder

As figure 3.18 demonstrates, convergence is happening and small changes are occurring while the amount of nodes is becoming of higher value, therefore there's only extra computational cost without much difference and the optimal meshing is the one explained aforementioned.

3.2.4 Conclusion

Using the setup explained in section 3.2.3, Velocity, Pressure and Vorticity Contours and the Stream line Pathlines can be obtained. As the computation is done, the Graphics section is ready for use. In the Contours section using Velocity contours, Velocity Magnitude and Vorticity Magnitude, and Pressure contour, Static pressure, figures 3.19 to 3.21 are derived. Furthermore using Pathlines for Velocity, Stream Function with 70 path skips and 500 steps, the Streamline Graphics are also yielded, demonstrated in figure 3.22.

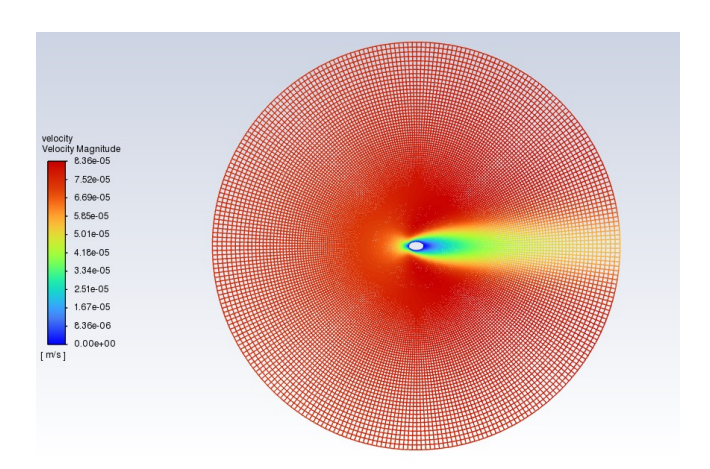


Figure 3.19: Velocity Contour for the Low Reynolds, Steady, Laminar simulation of flow against elliptical cylinder

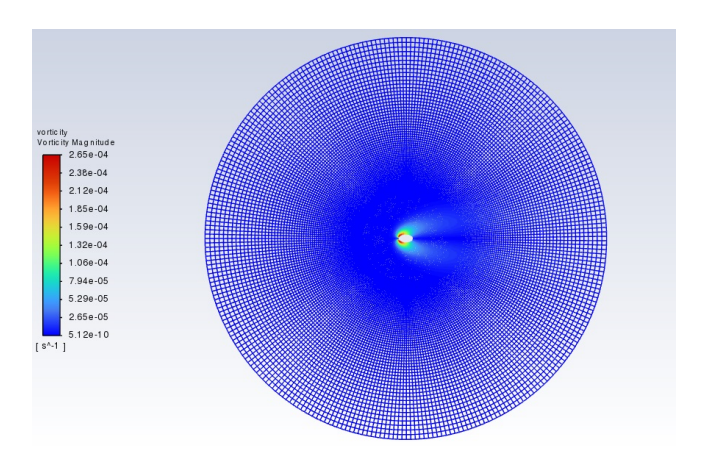


Figure 3.20: Vorticity Contour for the Low Reynolds, Steady, Laminar simulation of flow against elliptical cylinder

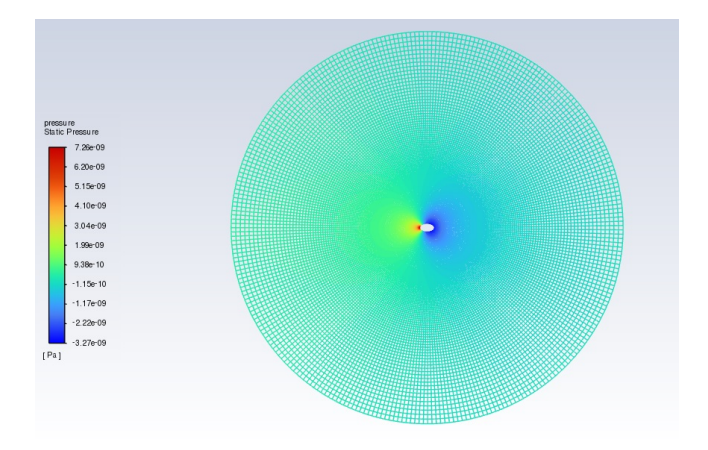


Figure 3.21: Pressure Contour for the Low Reynolds, Steady, Laminar simulation of flow against elliptical cylinder

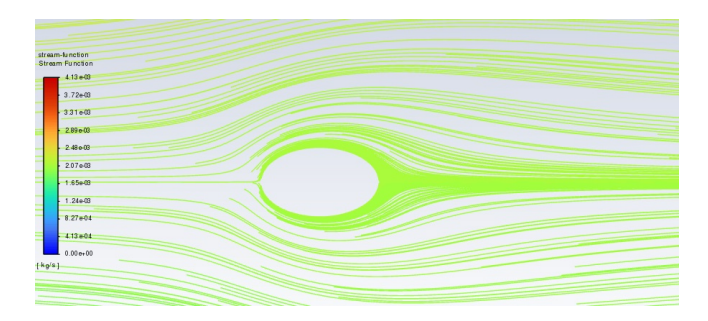


Figure 3.22: Streamline Graphics for the Low Reynolds, Steady, Laminar simulation of flow against elliptical cylinder

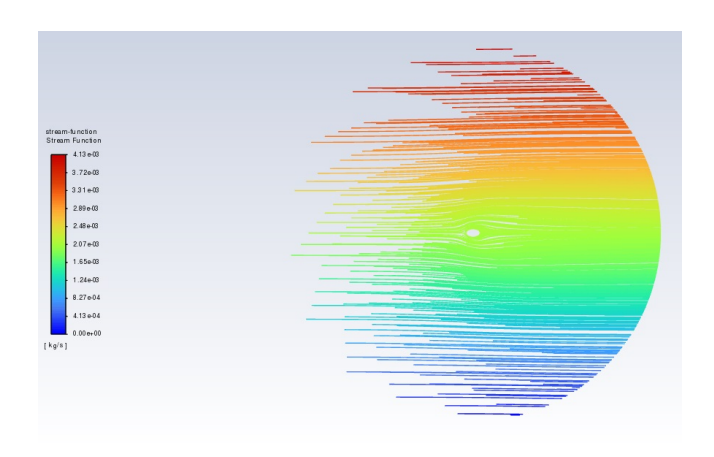


Figure 3.23: Streamline Graphics for the Low Reynolds, Steady, Laminar simulation of flow against elliptical cylinder

As expected for this regime with such low Reynolds, no separation has occurred and the flow has smoothly passed the cylinder with no wake regions as demonstrated in figure 3.22 and 3.23. In figure 3.23 it is also obvious that streamlines are not effected by the cylinder far from it and they are pretty straight as the original flow!

Like what was predicted also, the Velocity decreases around the cylindrical surface and there is a separation point infront and behind the cylinder at 0 and 180 degrees, as demonstrated in figure 3.19. It is also clear from figure 3.21 that in these previously mentioned points the pressure respectively reaches it's maximum and minimum values. At the end there are small vortices created due to the boundary layer conditions on the cylinder that are inconsiderable and are stronger closer to the cylinder over the inlet section as shown in figure 3.20. The growth of boundary layers is related to vorticity transport and for ow over the body, vorticity generated at the leading edge is advected by the ow, while diusing away from the body. furthermore explanation of this is given in appendix 7.3.1 and 7.3.2 by two articles.

The Lift Coefficient computed in this simulation, 0.0006 is inconsiderable whilst there is such larger Drag Coefficient computed, 4.291; Although the Lift Coefficient itself is more than the circular cylinder in a lower Reynolds, Considering it had less of a Reynolds value explains why we would have a little bit bigger vortices here surrounding the elliptical cylinder, but as it has a more streamlined body therefore it doesn't change drastically from the last part and is very close to it.

In this low Reynolds regime, the Drag Coefficient is mostly Frictional and has somewhat of a linear connection with the Reynolds number on a logarithmic scale! Checking this computation with the article given in appendix 7.1.2, there is some inconsiderable difference with the value found in the charts related to Newtonian fluids, with aspect ratio of 1.7 and Reynolds 5.

$$C_D = 4.158 \implies 3\% variance$$

The Report Definition charts for Lift and Drag Coefficients are demonstrated in figures 3.24 and 3.25.

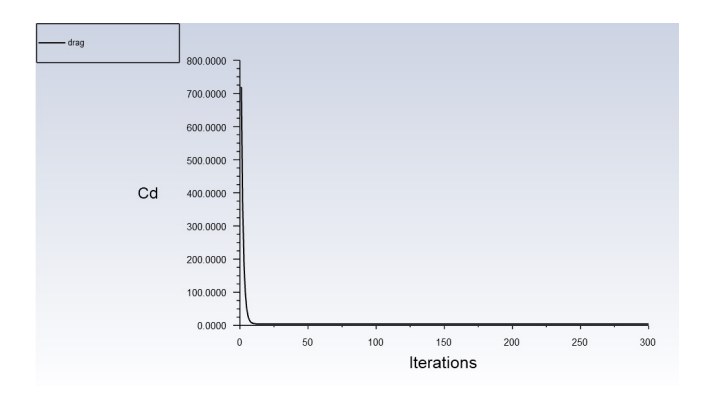


Figure 3.24: Drag Coefficient chart for the Low Reynolds, Steady, Laminar simulation of flow against elliptical cylinder

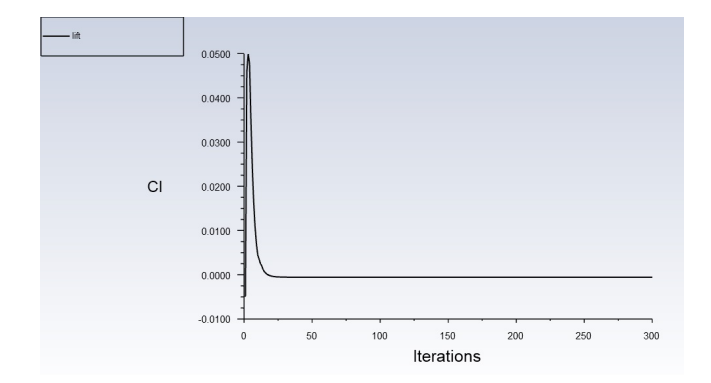


Figure 3.25: Lift Coefficient chart for the Low Reynolds, Steady, Laminar simulation of flow against elliptical cylinder

3.3 Moderate Reynolds regime, Elliptical section

3.3.1 Geometrical Settings

As the Geometry and Regime is the same and there's only a change in the Reynolds, the same Geometrical setting as elaborated in section 3.2.1 is applied!

3.3.2 Appropriate Meshing

Regarding the change in Reynolds, Changes in the mesh setting is required yet the overall pattern is exactly the same. An optimal proposed meshing is to use inflation with 7 layers of 1.2 growth rate alongside an Edge Sizing for the wall with a Number of Divisions, 500, to get the perfect boundary layer layout. Afterwise All Triangles method for the inner circular area around the ellipse and at last Structured Face Meshing using Quadrilaterals and alongside quad meshing, Edge Sizing for the two split lines with a growing bias type from the cylinders surface of the inner circular area to the surrounding surface, having a bias factor, 6, and a number of divisions, 40, has been used. The global meshing element size is set at 0.3 m. Furthermore changes in the meshing would be applied later to study mesh convergence. A schematic of the meshing quality is given in figure 3.26, having bigger elements than the meshing in section 3.2.2, it sure has lower quality!

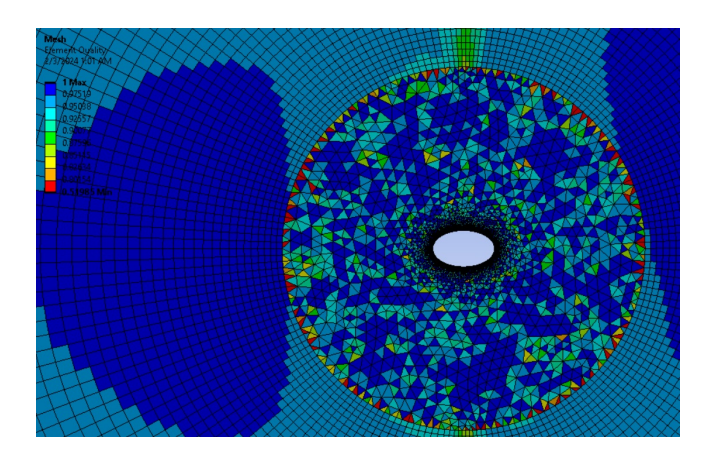


Figure 3.26: Appropriate meshing for the Moderate Reynolds, Steady, Laminar simulation of flow against elliptical cylinder

Of course the inlet, outlet, wall and fluid sections would be named using named selections option for each edge or surface, so that the simulation would go smoothly without problems. As elaborated in 3.2.2, O-type meshing around the ellipse is not a reasonable option considering the amount of nodes requiring computation change drastically although results are not much different, therefore less computational cost is desirable and O-type meshing will not be discussed.

3.3.3 Simulation

The simulation process is exactly the same as before, there's just the new inlet velocity of $3(10^{-4} \frac{m}{s})$ due to the new Reynolds.



Figure 3.27: Summary of setting up options for the Moderate Reynolds, Steady, Laminar simulation of flow against elliptical cylinder

Computation with such settings yields the Drag and Lift Coefficients charts demonstrated in figure 3.34 and 3.35 further in the text, yet here for verifying mesh convergence, the setup used for meshing in part 3.3.2, changes respectively upgrading the nodes, approximately computing the Drag coefficient with new node statistics 1.5 times the previous nodes each time. For this matter the Element size is made less each time and the Number of Divisions or Bias Factor for Edge Sizing is also increased, each multiplied or divide by $\sqrt{1.5}$!

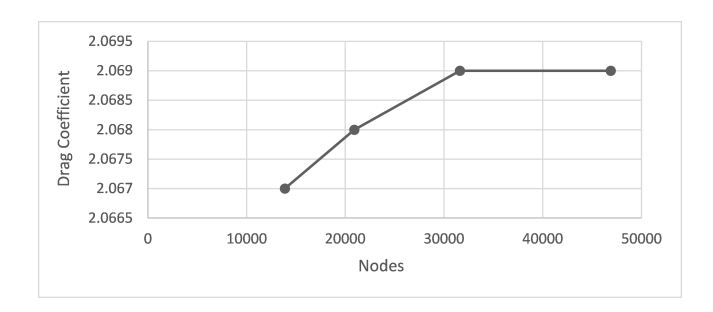


Figure 3.28: Mesh Convergence for the Moderate Reynolds, Steady, Laminar simulation of flow against elliptical cylinder

As figure 3.28 demonstrates, convergence is happening and small changes are occurring while the amount of nodes is becoming of higher value, therefore there's only extra computational cost without much difference and the optimal meshing is the one explained aforementioned.

3.3.4 Conclusion

Using the setup explained in section 3.3.3, Velocity, Pressure and Vorticity Contours and the Stream line Pathlines can be obtained. As the computation is done, the Graphics section is ready for use. In the Contours section using Velocity contours, Velocity Magnitude and Vorticity Magnitude, and Pressure contour, Static pressure, figures 3.29 to 3.31 are derived. Furthermore using Pathlines for Velocity, Stream Function with 70 path skips and 500 steps, the Streamline Graphics are also yielded, demonstrated in figure 3.32.

^{*}Any other options needed is set as the software's default

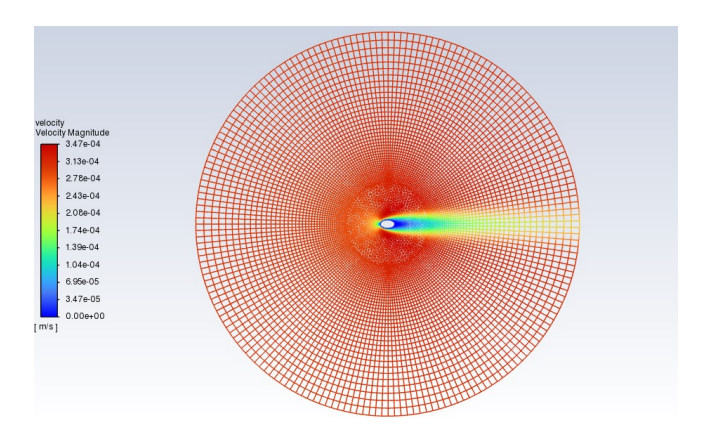


Figure 3.29: Velocity Contour for the Moderate Reynolds, Steady, Laminar simulation of flow against elliptical cylinder

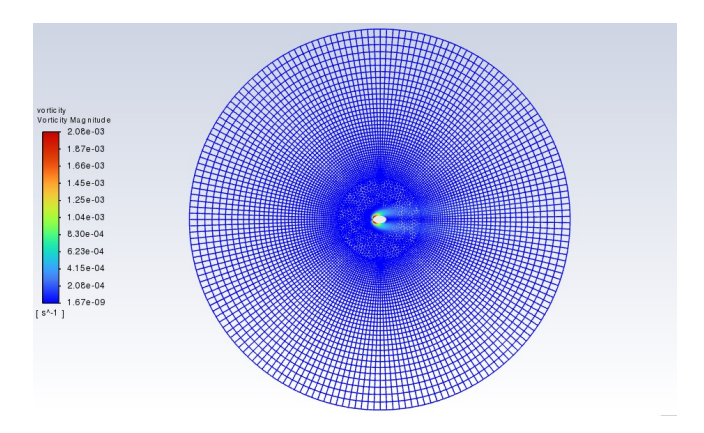


Figure 3.30: Vorticity Contour for the Moderate Reynolds, Steady, Laminar simulation of flow against elliptical cylinder

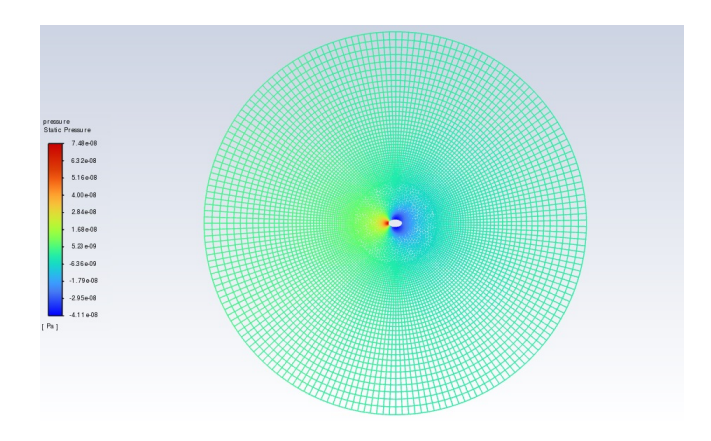


Figure 3.31: Pressure Contour for the Moderate Reynolds, Steady, Laminar simulation of flow against elliptical cylinder

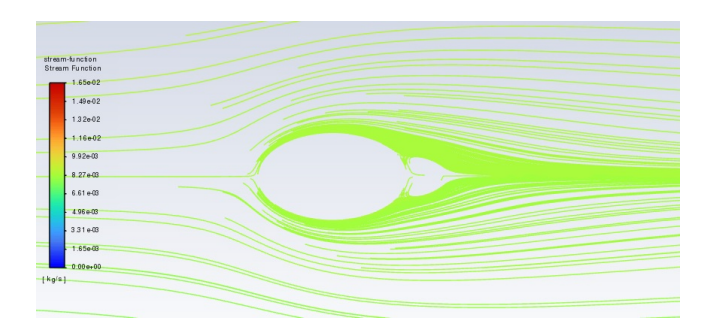


Figure 3.32: Streamline Graphics for the Moderate Reynolds, Steady, Laminar simulation of flow against elliptical cylinder

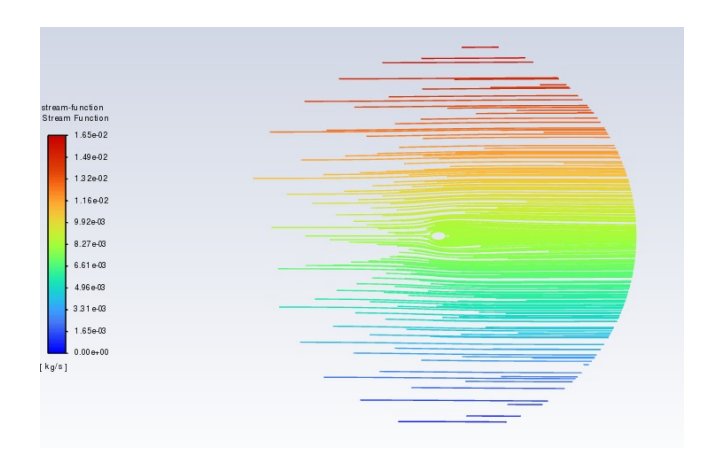


Figure 3.33: Streamline Graphics for the Moderate Reynolds, Steady, Laminar simulation of flow against elliptical cylinder

As expected for this regime with moderate Reynolds, attached and symmetrical separation has occurred meaning the wake region is created behind the cylinder but it doesn't move away with the flow and is stuck besides the cylinder as demonstrated in figure 3.32 and 3.33. In figure 3.33 it is also obvious that streamlines are not effected by the cylinder far from it and they are pretty straight as the original flow! As it's explicitly analyzed in the article shared in section 7.3.3 (Section 3.1 in article), two counter-rotating symmetric recirculation regions are expected to develop on each side of the wake as demonstrated by the simulation in figure 3.32! Like what was predicted also, the Velocity decreases around the cylindrical surface and there is a separation point infront and behind the cylinder but unlike section 3,2,4, the wake region has its effect on the velocity contour as demonstrated in figure 3.29, We can see how the region having lower velocities behind the cylinder is increasing as well as in figure 3.31 where the vortices identified in figure 3.32 are distinct as they are bigger than before. It is also clear from figure 3.31 that in these previously mentioned stagnation points the pressure respectively reaches it's maximum and minimum values. At the end there are small vortices created due to the boundary layer conditions on the cylinder that are inconsiderable and are stronger closer to the cylinder over the inlet section as shown in figure 3.30. The growth of boundary layers is related to vorticity transport and for ow over the body, vorticity generated at the leading edge is advected by the ow, while diusing away from the body. furthermore explanation of this is given in appendix 7.3.1 and 7.3.2 by two articles.

The Lift Coefficient computed in this simulation, 0.001 is inconsiderable whilst there is such larger Drag Coefficient computed, 2.067; Although the Lift Coefficient itself is more than the cylinder in a lower Reynolds, Considering it had less of a Reynolds value explains why we

would have a little bit bigger vortices here surrounding the elliptical cylinder, attached and symmetrical vortices in comparison with no vortices in lower Reynolds regime.

Checking this computation with the article given in appendix 7.1.2, there is some inconsiderable difference with the value found in the charts related to Newtonian fluids, with aspect ratio of 1.7 and Reynolds 20.

$$C_D = 2.509 \implies 17\% variance$$

The Report Definition charts for Lift and Drag Coefficients are demonstrated in figures 3.34 and 3.35.

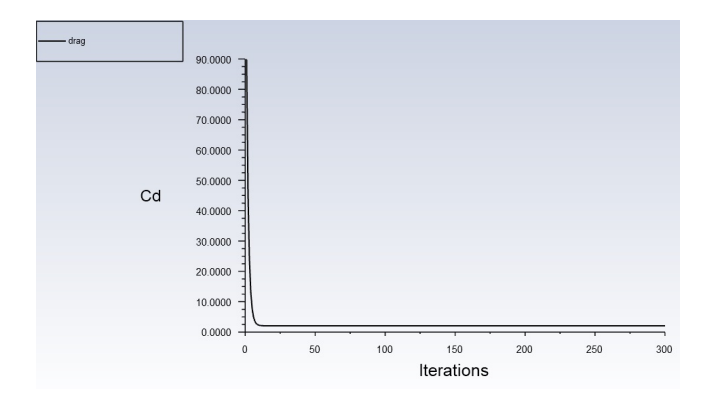


Figure 3.34: Drag Coefficient chart for the Moderate Reynolds, Steady, Laminar simulation of flow against elliptical cylinder

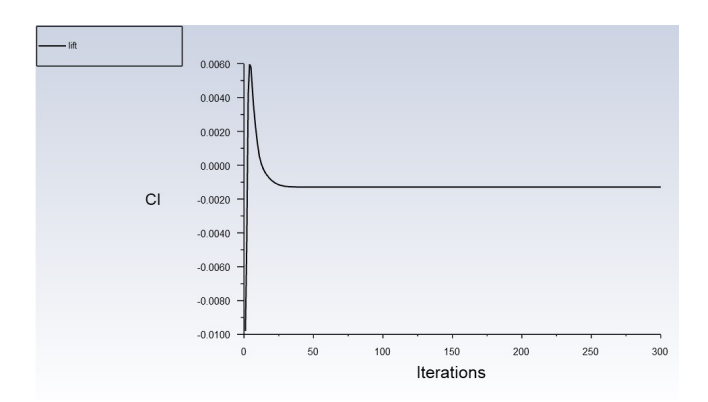


Figure 3.35: Lift Coefficient chart for the Moderate Reynolds, Steady, Laminar simulation of flow against elliptical cylinder

4. Transient, Laminar vortex shedding

For the third and fourth configurations discussed in this part, a rather transient, laminar flow is studied, given various Reynolds regimes. With the help of fluid simulation software, ANSYS Fluent, each configuration is met with its own particular geometrical settings specifying the domain sufficient for computation, furthermore followed by its appropriate meshing style taking into account the flow regime. Afterwards it's setup for computation to yield the desired parameters and be analogized with the related articles presented in chapter 7. As there are wakes expected, animations of these wakes are also obtained.

4.1 Moderate Reynolds regime, Elliptical section

4.1.1 Geometrical Settings

As the Geometry is the same for this Moderate Reynolds flow and the one discussed in section 3.3, and there's only a change in the Reynolds, the same Geometrical setting as elaborated in section 3.2.1 is applied!

4.1.2 Appropriate Meshing

For this configuration, as we have a larger Reynolds number and would prefer a higher quality solution to obtain great a great animation of the vortices behind the body and the wake region, the meshing applied is the same meshing used in section 3.2.2.

4.1.3 Simulation

As the simulation is approached having specified the proper geometry and meshing, for computation, the option double precision is checked before launching the simulation and also 4 solver processes are used in order to get the desired results.

The modified settings for the configuration given in Table 2.1; Pressure Based, Transient solver, Viscous(laminar) in Models, air as specific fluid in Cell Zone Conditions, inlet velocity set $45(10^{-4}) \frac{m}{s}$ regarding the given Reynolds, 300, measured by equation 2.1 and Velocity Specification Method, Magnitude and Direction, and finally setting the Reference value as the inlet velocity, is applied.

Afterwards the solution method is set as coupled with the gradient settings set as the Least Squares Cell Based option considering it's the one choice with the optimal computational cost, and furthermore setting the Pressure's equation interpolation as second order and the Momentum's equation as second order upwind.

Following up we set up two report definitions for the drag and lift coefficients, using the right force vectors, perpendicular to stream for lift and parallel to stream for drag, making sure the wall zone is well selected.

As it is desired to have the meshing converge we take the Check Convergence options in Residual Monitors off and set enough time steps and iterations to reach convergence ourselves.

Eventually using Standard Initialization, recommended for transient flows the initialization is done computing from inlet. For Calculations, as we are aiming to have mesh convergence, different Number of Time Steps and Time Step Durations are applied to get the best results. Alongside all these settings, in Calculation Activities, Auto Save for every 5 Time Steps is also launched, helping us achieve the desired animations later on.

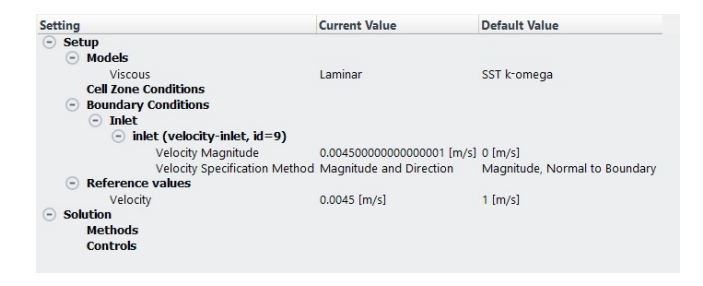


Figure 4.1: Summary of setting up options for the Moderate Reynolds, Transient, Laminar simulation of flow against elliptical cylinder

Calculating the Strouhal number from equation 2.2, with the configuration's specific conditions met and setting the Strouhal number about 0.2 derived from the article shared in appendix 7.1.3 (Figure 11), the Time Step Duration must be 1111 s. Computing for three different orders 1000 s, 100 s and 10 s with Number of Time Steps set as 225 (5 times across the Surrounding area), the scaled residuals charts are obtained as below.

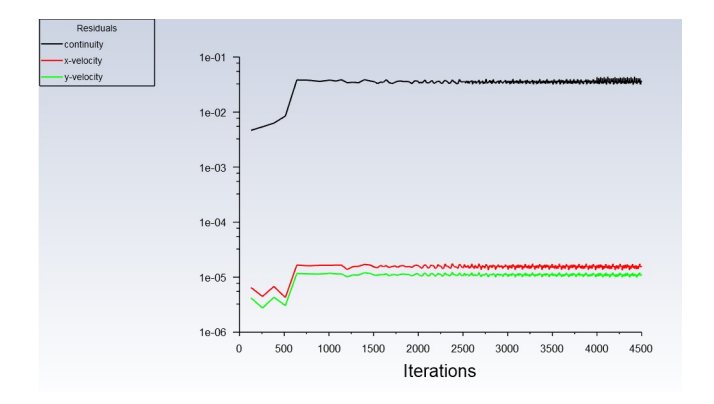


Figure 4.2: Scaled Residuals for the Moderate Reynolds, Transient, Laminar simulation of flow against elliptical cylinder (Time Step Duration = 1000 s)

^{*}Any other options needed is set as the software's default

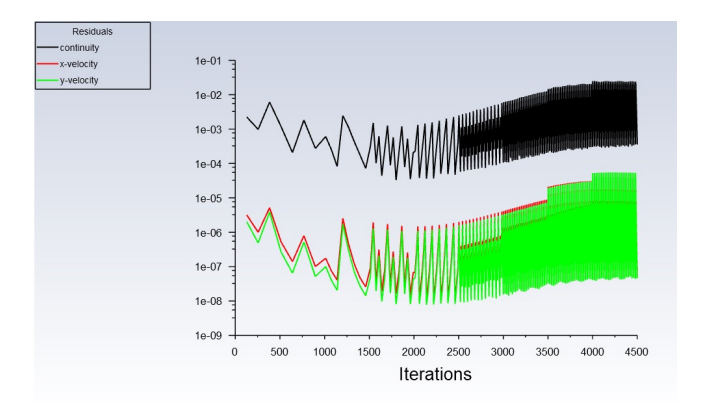


Figure 4.3: Scaled Residuals for the Moderate Reynolds, Transient, Laminar simulation of flow against elliptical cylinder (Time Step Duration = 100 s)

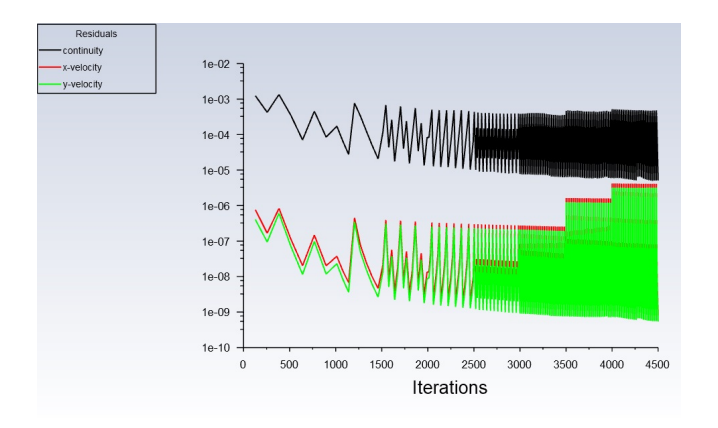


Figure 4.4: Scaled Residuals for the Moderate Reynolds, Transient, Laminar simulation of flow against elliptical cylinder (Time Step Duration = 10 s)

As it can be concluded from figure 4.2 to 4.4, the optimal Time Step Duration is 100 s, that yields a converged chart for the residuals (the oscillation domain becoming of more) compared to a Time Step Duration of higher order and also has less computational cost!, it's also closer to the desired Time Step Duration leading to a Strouhal number of O(0.1). This Time Step Duration also yields great graphics for the streamlines that perfectly show the wake region behind the elliptical surface.

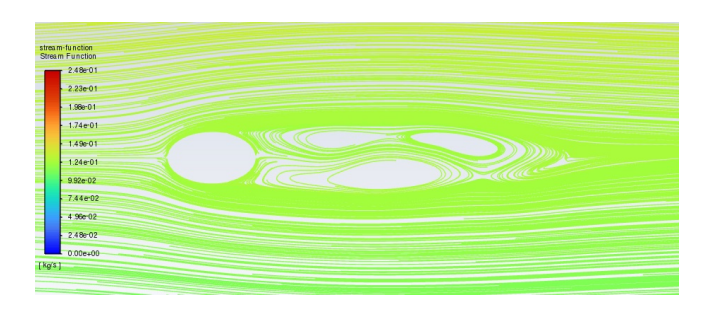


Figure 4.5: Streamline Graphics for the Moderate Reynolds, Transient, Laminar simulation of flow against elliptical cylinder (Time Step Duration = 1000 s)

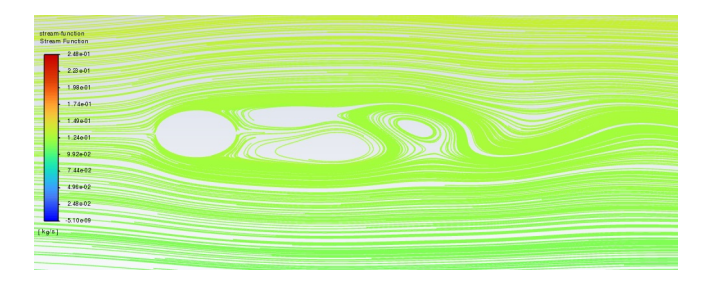


Figure 4.6: Streamline Graphics for the Moderate Reynolds, Transient, Laminar simulation of flow against elliptical cylinder (Time Step Duration = 100 s)

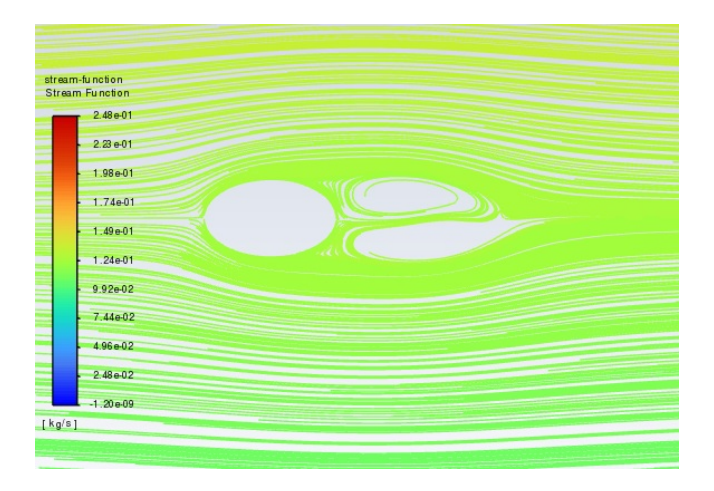


Figure 4.7: Streamline Graphics for the Moderate Reynolds, Transient, Laminar simulation of flow against elliptical cylinder (Time Step Duration = 10 s)

4.1.4 Conclusion

Using the setup explained in section 4.1.3, Velocity, Pressure and Vorticity Contours and the Stream line Pathlines can be obtained. As the computation is done, the Graphics section is ready for use. In the Contours section using Velocity contours, Velocity Magnitude and Vorticity Magnitude, and Pressure contour, Static pressure, figures 4.8 to 4.10 are derived. Furthermore using Pathlines for Velocity, Stream Function with 50 path skips and 500 steps, the Streamline Graphics are also yielded, demonstrated in figure 4.11.

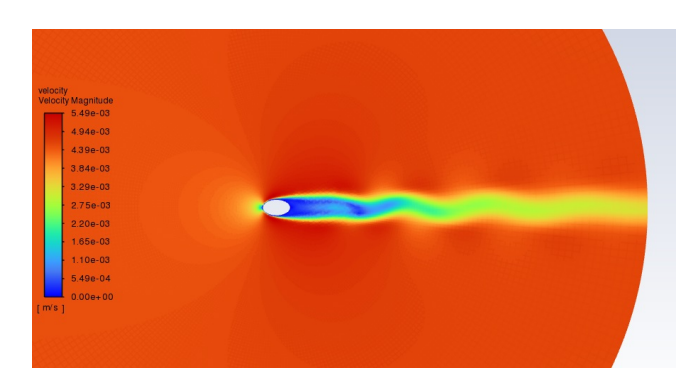


Figure 4.8: Velocity Contour for the Moderate Reynolds, Transient, Laminar simulation of flow against elliptical cylinder



Figure 4.9: Vorticity Contour for the Moderate Reynolds, Transient, Laminar simulation of flow against elliptical cylinder

*Vorticity contour has been modified demonstrating areas with vortices stronger that 0.001 s^{-1} and weaker than 0.15 s^{-1}

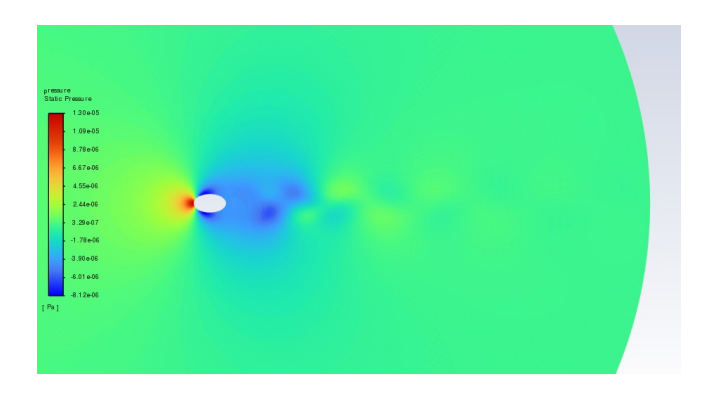


Figure 4.10: Pressure Contour for the Moderate Reynolds, Transient, Laminar simulation of flow against elliptical cylinder

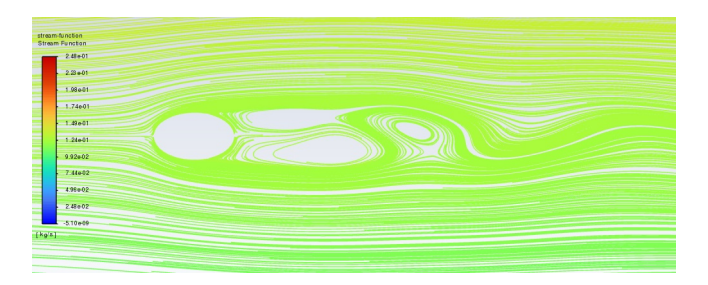


Figure 4.11: Streamline Graphics for the Moderate Reynolds, Transient, Laminar simulation of flow against elliptical cylinder

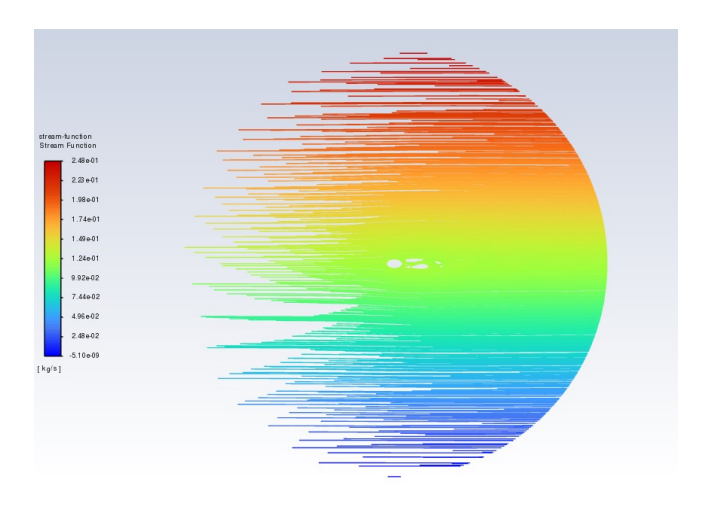


Figure 4.12: Streamline Graphics for the Moderate Reynolds, Transient, Laminar simulation of flow against elliptical cylinder

As there is a Transient configuration, the regime is naturally unsteady, separations are obvious in the contours above and the streamline graphics. The wake region's length is increased compared to the the previously analyzed regimes. In this Transient regime as the Reynolds has passed it's critical value, Vortices have movement downstream and oscillations of the separated region appear in the wake and the flow regime initiates periodic oscillations, as is demonstrated by figure 4.11, noting that again far from the bluff body, the streamlines are barely affected by the body and are straight lines as they should be! Consequently, large and spanwise homogeneous vortices are shed from the rear surface and transported downstream. The transition to vortex shedding occurs when the recirculation region which had been formed behind the circular cylinder in the steady flow regime is opened, and immediate fluid alleyways are penetrated into the recirculation region. furthermore explanation is provided in the article in section 7.3.3 (Sections 3.1 and 3.2 of the article).

Regarding the Velocity Contour of figure 4.8, it is well obvious that a stagnation point is set at 0 degrees on the elliptical surface and the other stagnation points are at about 80 degrees, considering it is a laminar flow this is totally reasonable and compatible with theory! it is obvious how the velocity decreases moving towards the initial stagnation point and afterwards the flow gains more velocity and momentum, yet eventually reaching a point where it cannot confront the adverse gradient it is facing, it disparts the bluff body's surface, leaving wake regions behind as well as causing large vortices behind the bluff body as demonstrated by figure 4.9. It is clear in figure 4.9 how initially when the flow hits the body a large vorticity is created as explained before in sections 3.3.4 and 3.2.4, due to large inlet velocity suddenly reaching the stagnation point. but the vortices remain powerful in this case with higher Reynolds value, moving across the flow behind the body, as they are moving downstream the kinetic energy regarding these vortices slowly converts into heat and they disappear.

A better Streamline Graphics has also been obtained by increasing the Number of Time Steps to 550 (10 times across the Surrounding area), and is demonstrated in figure 4.13. This phenomenon is better explained by the velocity contour animation shared in appendix 7.4.1, using the same settings as explained now.

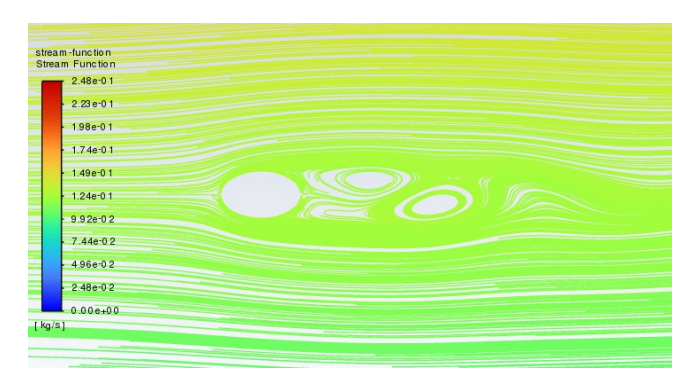


Figure 4.13: Better Streamline Graphics for the Moderate Reynolds, Transient, Laminar simulation of flow against elliptical cylinder

Eventually the pressure contour also is explicit about the maximum pressure at the initial stagnation point and the decreased pressure at the other points.

The Drag Coefficient Computed is 0.724 which is pretty much larger than the Lift Coefficient, 0.002, since there's a symmetrical geometry, no lift is expected as the simulation agrees, and since there's a Transient regime with Moderate Reynolds the Drag Coefficient is theoretically Expected to Decrease comparing to the previous configurations, which this also is obvious in the simulation.

It is ofcourse worthy of mention that the simulation's computation agrees with experimental work done in article 7.3.3 (Figure 20, Section 4.1.1).

The Report Definitions Charts for Lift and Drag Coefficients are demonstrated in figures 4.14 and 4.15.

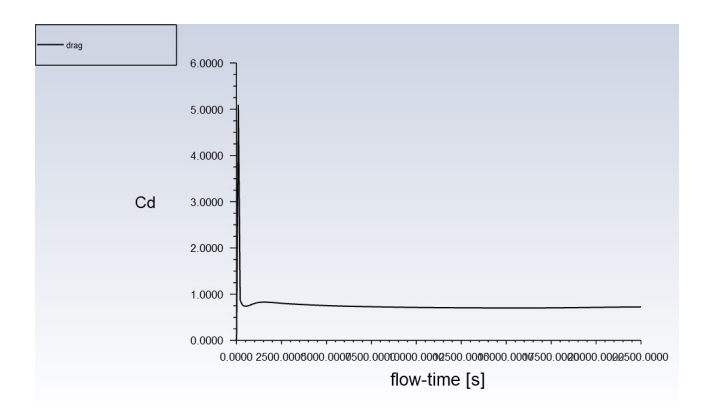


Figure 4.14: Drag Coefficient chart for the Moderate Reynolds, Transient, Laminar simulation of flow against elliptical cylinder

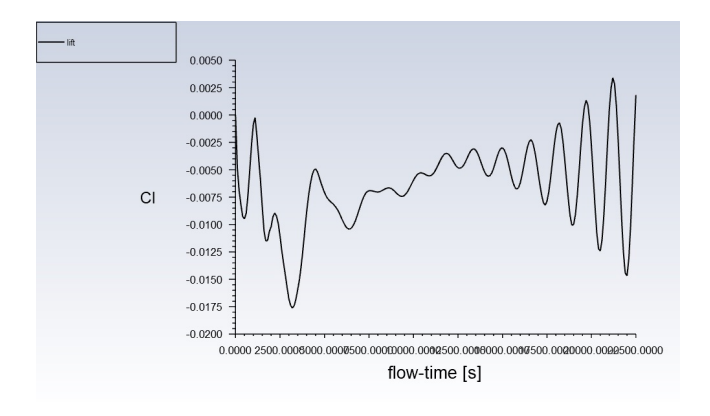


Figure 4.15: Lift Coefficient chart for the Moderate Reynolds, Transient, Laminar simulation of flow against elliptical cylinder

Studying the chart shown in figure 4.15 furthermore, the oscillation period (at the end of the chart) can be determined which here is nearly 1500 s. Calculating the Strouhal number from equation 2.2, using this frequency obtained yields the Strouhal number of the same order as assumed beforehand.

$$St = \frac{1500^{-1}(1)}{0.0045} = 0.15 O(0.1) \checkmark$$

Checking this Strouhal number with the experimental results shared in the article of section 7.1.3, we can have an idea of the variance (Obtaining the experimental data from figure 11).

$$St = 0.19 \implies 20\% variance$$

4.2 High Reynolds regime, Elliptical section

4.2.1 Geometrical Settings

As the Geometry is the same for this High Reynolds flow and the one discussed in section 4.1, and there's only a change in the Reynolds, the same Geometrical setting as elaborated in section 4.1.1 is applied!

4.2.2 Appropriate Meshing

For this configuration, as we have a larger Reynolds number and would prefer a higher quality solution to obtain great a great animation of the vortices behind the body and the wake region, the meshing applied is the same meshing used in section 4.1.2.

4.2.3 Simulation

The simulation process is exactly the same as before, there's just the new inlet velocity of $135(10^{-4}) \frac{m}{s}$ due to the new Reynolds.

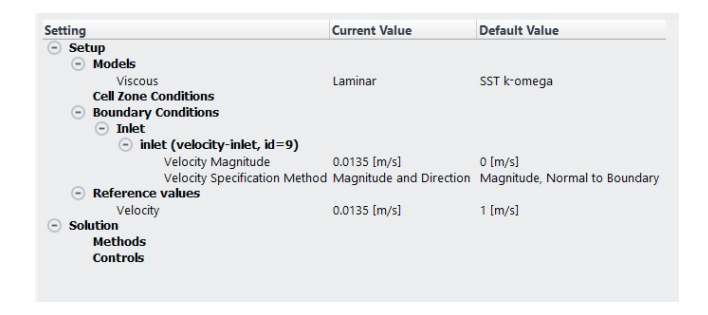


Figure 4.16: Summary of setting up options for the High Reynolds, Transient, Laminar simulation of flow against elliptical cylinder

Calculating the Strouhal number from equation 2.2, with the configuration's specific conditions met and also assuming Strouhal number to be of O(0.1) order, the Time Step Duration must be 370 s. Computing for two different orders 300 s and 30 s with Number of Time Steps set as 225 (5 times across the Surrounding area), the scaled residuals charts are obtained as below.

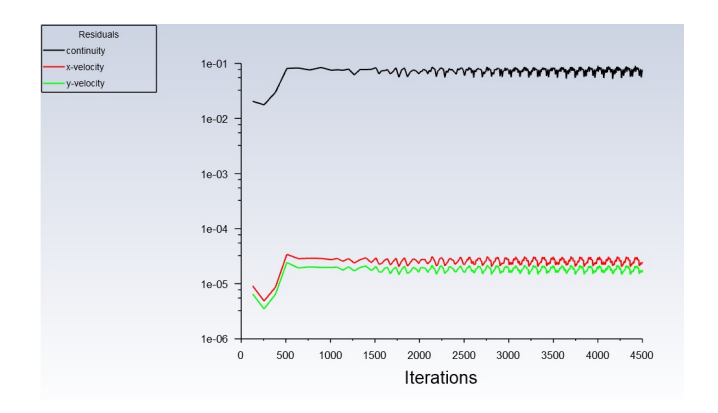


Figure 4.17: Scaled Residuals for the High Reynolds, Transient, Laminar simulation of flow against elliptical cylinder (Time Step Duration = 300 s)

^{*}Any other options needed is set as the software's default

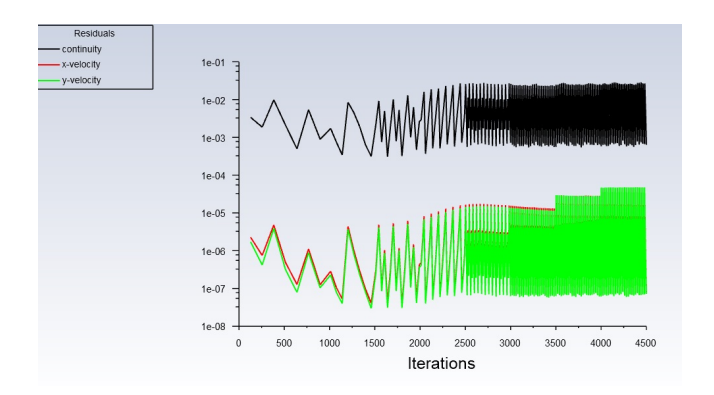


Figure 4.18: Scaled Residuals for the High Reynolds, Transient, Laminar simulation of flow against elliptical cylinder (Time Step Duration = 30 s)

As it can be concluded from figure 4.17 and 4.18, the optimal Time Step Duration is 30 s, that yields a converged chart for the residuals (the oscillation domain becoming of more) compared to a Time Step Duration of higher order and also has less computational cost! This Time Step Duration also yields great graphics for the streamlines that perfectly show the wake region behind the elliptical surface.

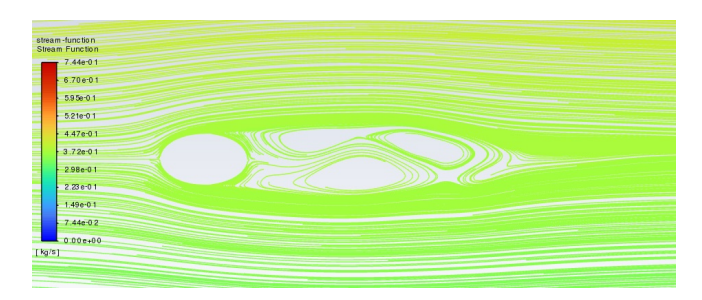


Figure 4.19: Streamline Graphics for the High Reynolds, Transient, Laminar simulation of flow against elliptical cylinder (Time Step Duration = 300 s)

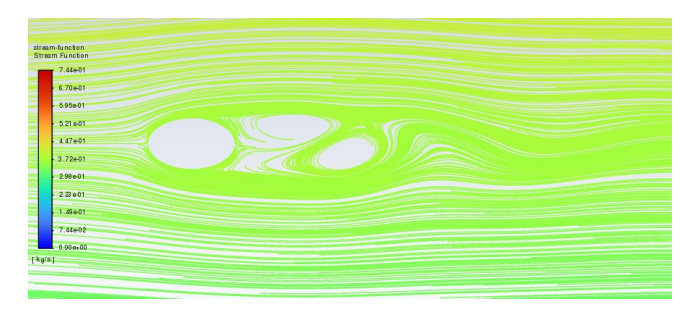


Figure 4.20: Streamline Graphics for the High Reynolds, Transient, Laminar simulation of flow against elliptical cylinder (Time Step Duration = 30 s)

4.2.4 Conclusion

Using the setup explained in section 4.2.3, Velocity, Pressure and Vorticity Contours and the Stream line Pathlines can be obtained. As the computation is done, the Graphics section is ready for use. In the Contours section using Velocity contours, Velocity Magnitude and Vorticity Magnitude, and Pressure contour, Static pressure, figures 4.21 to 4.23 are derived. Furthermore using Pathlines for Velocity, Stream Function with 50 path skips and 500 steps, the Streamline Graphics are also yielded, demonstrated in figure 4.24.

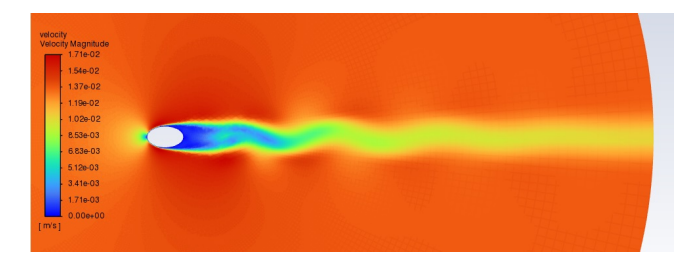


Figure 4.21: Velocity Contour for the High Reynolds, Transient, Laminar simulation of flow against elliptical cylinder



Figure 4.22: Vorticity Contour for the High Reynolds, Transient, Laminar simulation of flow against elliptical cylinder

*Vorticity contour has been modified demonstrating areas with vortices stronger that 0.001 s^{-1} and weaker than 0.5 s^{-1}

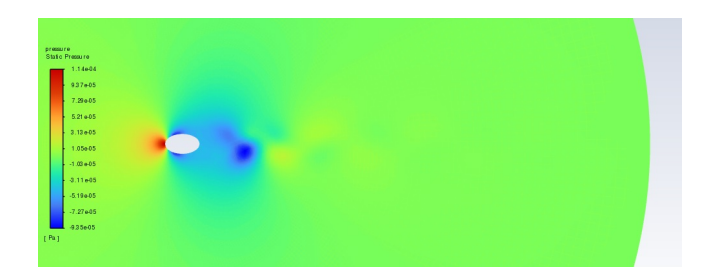


Figure 4.23: Pressure Contour for the High Reynolds, Transient, Laminar simulation of flow against elliptical cylinder

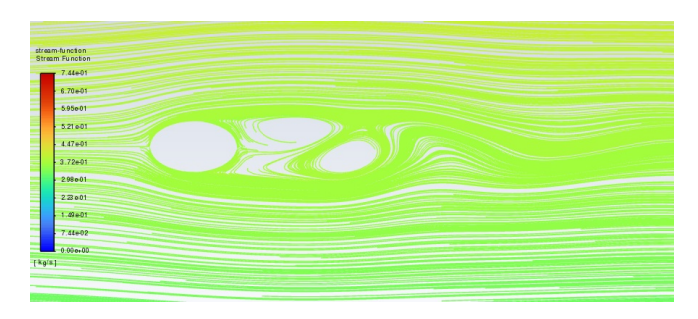


Figure 4.24: Streamline Graphics for the High Reynolds, Transient, Laminar simulation of flow against elliptical cylinder

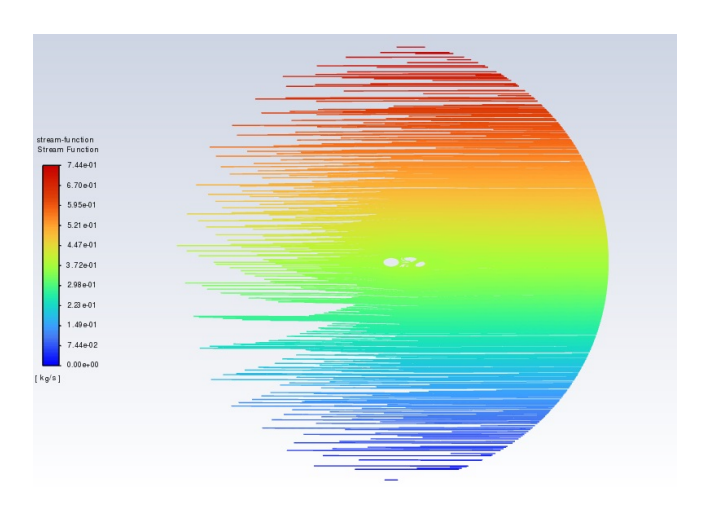


Figure 4.25: Streamline Graphics for the High Reynolds, Transient, Laminar simulation of flow against elliptical cylinder

As there is a Transient configuration, the regime is naturally unsteady, separations are obvious in the contours above and the streamline graphics. The wake region's length is increased compared to the the previously analyzed regimes. In this Transient regime as the Reynolds has passed it's critical value, Vortices have movement downstream and oscillations of the separated region appear in the wake and the flow regime initiates periodic oscillations, as is demonstrated by figure 4.24, noting that again far from the bluff body, the streamlines are barely affected by the body and are straight lines as they should be! Consequently, large and spanwise homogeneous vortices are shed from the rear surface and transported downstream. The transition to vortex shedding occurs when the recirculation region which had been formed behind the circular cylinder in the steady flow regime is opened, and immediate fluid alleyways are penetrated into the recirculation region. furthermore explanation is provided in the article in section 7.3.3 (Sections 3.1 and 3.2 of the article).

Regarding the Velocity Contour of figure 4.21, it is well obvious that an initial stagnation point is set at 0 degrees on the elliptical surface like the previous section 4.1.4, yet the other stagnation points seem to have moved a little bit further forward as the Reynolds has been increased and the transition is getting closer to a turbulent regime flow, therefore this is totally reasonable and compatible with theory! it is obvious how the velocity decreases moving towards the initial stagnation point and afterwards the flow gains more velocity and momentum, yet eventually reaching a point where it cannot confront the adverse gradient it is facing, it disparts the bluff body's surface, leaving wake regions behind as well as causing larger vortices behind than the previous section, as demonstrated by figure 4.22. It is clear in figure 4.22 how initially when the flow hits the body a large vorticity is created as explained before in sections 3.3.4 and 3.2.4, due to large inlet velocity suddenly reaching the stagnation point. but the vortices remain powerful in this case with higher Reynolds value, moving across the flow behind the body, as they are moving downstream the kinetic energy regarding these vortices slowly converts into heat and they disappear.

A better Streamline Graphics has also been obtained by increasing the Number of Time Steps to 550 (10 times across the Surrounding area), and is demonstrated in figure 4.26. This phenomenon is better explained by the velocity contour animation shared in appendix 7.4.2, using the same settings as explained now, as it is demonstrated in the animation, larger wake region is created in this configuration compared to the last one considering it's higher Reynolds value, the vortices are of bigger quantity and vortex shedding is obvious across the flow field behind the cylinder.

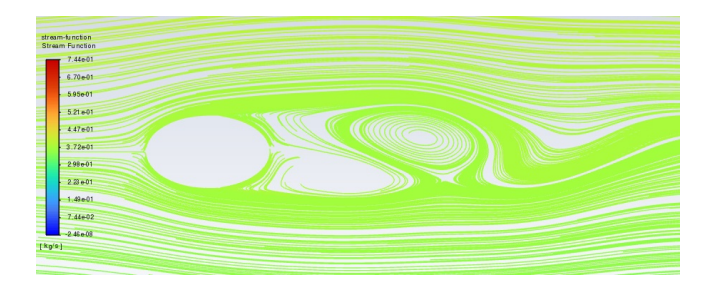


Figure 4.26: Better Streamline Graphics for the High Reynolds, Transient, Laminar simulation of flow against elliptical cylinder

Eventually the pressure contour also is explicit about the maximum pressure at the initial stagnation point and the decreased pressure at the other points. In the contour shared in figure 4.23, there is a point further from the cylinder where the pressure has become very low causing the Lift Coefficient explained later on in the text to become more than the previous section. The formation of this point having a low pressure is related to the wake region and the vortex seen in figure 4.24, regarding it's higher velocity as is shown in figure 4.21 and it's vorticity in figure 4.22, it can be concluded that compared to it's surroundings it has a bigger value of velocity therefore (considering it is far away from the cylinder which is right and approaching it with potential theory solution) it has less pressure.

The Drag Coefficient Computed is 0.616 which is pretty much larger than the Lift Coefficient, 0.02, since there's a symmetrical geometry, no Lift of great quantity is expected as the simulation agrees, yet it still has differences with the previous section considering larger wake regions and vortices are being analyzed as explained above. Since there's a Transient regime with High Reynolds the Drag Coefficient is theoretically Expected to Decrease comparing to the previous configurations, which this also is obvious in the simulation.

It is ofcourse worthy of mention that the simulation's computation agrees with experimental work done in article 7.3.3 (Figure 14, Section 3.3).

The Report Definitions Charts for Lift and Drag Coefficients are demonstrated in figures 4.27 and 4.28.

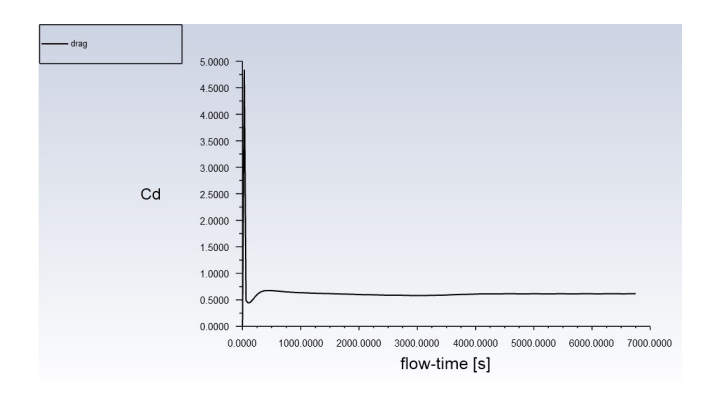


Figure 4.27: Drag Coefficient chart for the High Reynolds, Transient, Laminar simulation of flow against elliptical cylinder

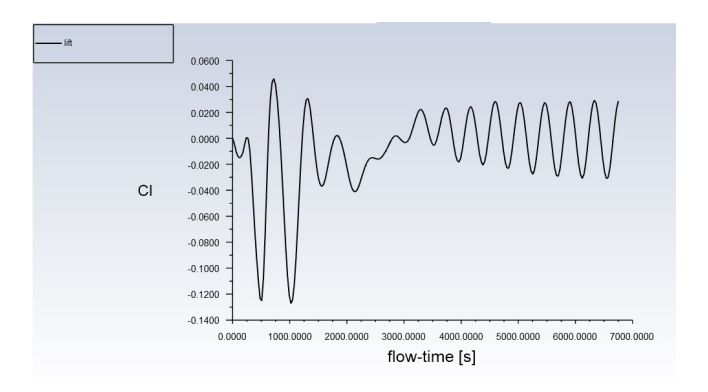


Figure 4.28: Lift Coefficient chart for the High Reynolds, Transient, Laminar simulation of flow against elliptical cylinder

Studying the chart shown in figure 4.26 furthermore, the oscillation period (at the end of the chart) can be determined which here is nearly 500 s. Calculating the Strouhal number from equation 2.2, using this frequency obtained yields the Strouhal number of the same order as assumed beforehand.

$$St = \frac{500^{-1}(1)}{0.0135} = 0.15 O(0.1) \checkmark$$

Checking this Strouhal number with the experimental results shared in the articles of section 7.3.4, to 7.3.7, we can have an idea of the variance, regarding the articles with the idea that an ellipse with aspect ratio of 1.7 is very much more streamlined, it can be concluded that the Strouhal number calculated is of the right order and quantity. (The articles are related to polygon or circular cylinders or rather elliptical cylinders with small aspect ratios, resulting in higher Strouhal numbers considering the higher vortex shedding frequencies).

5. Steady, Turbulent vortex shedding

5.1 High Reynolds regime, Elliptical section

5.1.1 Geometrical Settings

As the Geometry is the same for this very high Reynolds flow and the one discussed in section 3.3, and there's only a change in the Reynolds, the same Geometrical setting as elaborated in section 3.2.1 is applied!

5.1.2 Appropriate Meshing

For this configuration, as we have a larger Reynolds number and would prefer a higher quality solution to obtain great a great animation of the vortices behind the body and the wake region, the meshing applied is the same meshing setting used in section 4.2.2, but since the configuration is that of a Turbulent flow, it is important to have close wall distance over the first few cells near the cylinder. In order to achieve this, changes have been applied to the meshing sizing. To begin with the global Element Size has been changed to 0.1 m, the inflation Number of layers has been increased to 12 layers with Growth Rate set at 1.4 and maximum Thickness of 0.1 m (as the global Element Size settings); With that being said the initial wall distance is about 0.0018 m, which results in y+ equal to 1 (Calculated by CFD online). Other changes are Edge Sizings being modified to, wall edge Number of Divisions changed to 3000! and split line edges Number of Divisions changed to 150, with a Bias Factor, 6. With this configuration the overall nodes are about 134000!

A schematic of the meshing is given in figure 5.1.

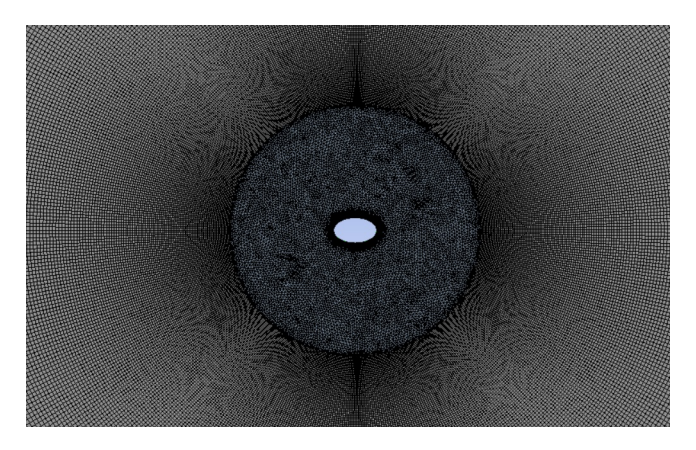


Figure 5.1: Appropriate meshing for the High Reynolds, Steady, Turbulent simulation of flow against elliptical cylinder

Of course the inlet, outlet, wall and fluid sections would be named using named selections option for each edge or surface, so that the simulation would go smoothly without problems. The mesh Element Quality is also demonstrated in the figure below.

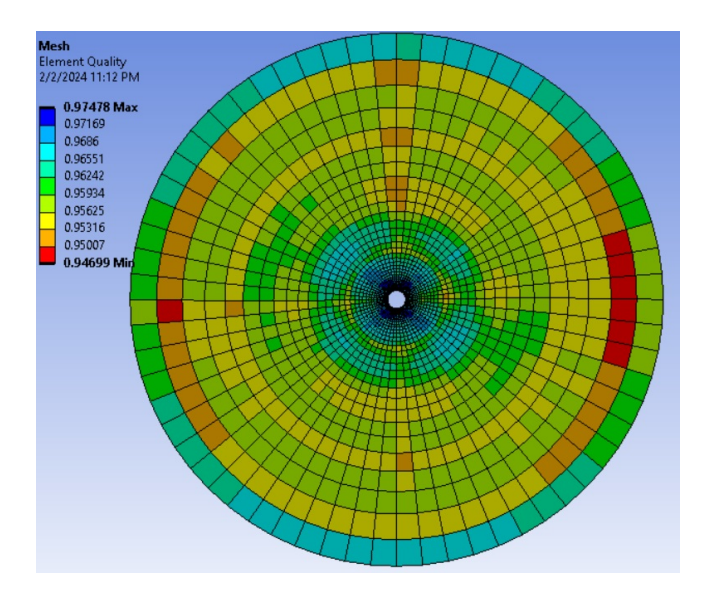


Figure 5.2: Mesh Element Quality for the High Reynolds, Steady, Turbulent simulation of flow against elliptical cylinder

It is worthy of mention that along Simulation, changes may be needed to be applied over the meshing for it to converge and yield correct responses, therefore sizings mentioned above might be changed and affected by the Simulation's method!

5.1.3 Simulation

As the simulation is approached having specified the proper geometry and meshing, for computation, the option double precision is checked before launching the simulation and also 4 solver processes are used in order to get the desired results.

The modified settings for the configuration given in Table 2.1; Pressure Based, Steady solver, air as specific fluid in Cell Zone Conditions, inlet velocity set $1.5 \frac{m}{s}$ regarding the given Reynolds, 100000, measured by equation 2.1 and Velocity Specification Method, Magnitude and Direction, and finally setting the Reference value as the inlet velocity, is applied, One changing setting is the model used for computation, as there are many models including, k-epsilon, k-omega,

- 1 k-epsilon (Standard)
- 2 k-epsilon (Realizable)
- 3 k-omega (Standard)
- 4 Transition (SST)
- 5 Reynolds Stress

Table 5.1: Turbulent methods used

Transition SST and etc. In this project as the computational cost is important, the four models above are used for Computation each time, making sure the Enhanced Wall Treatment and Pressure Gradient Effects options are checked whenever needed.

Afterwards the solution method is set as coupled with the gradient settings set as the Least Squares Cell Based option considering it's the one choice with the optimal computational cost, and furthermore setting the Pressure's equation interpolation as second order and the Momentum's equation as second order upwind.

Following up we set up two report definitions for the Drag Force and Lift Coefficients, using the right force vectors, perpendicular to stream for lift and parallel to stream for drag, making sure the wall zone is well selected.

As it is desired to have the meshing converge we take the Check Convergence options in Residual Monitors off and set enough iterations to reach convergence ourselves.

Eventually using Hybrid Initialization, recommended for steady flows the initialization is done and using 200 iterations the simulation can be done.

Mesh Convergence issues are not to be discussed in this project yet as it has been mentioned before, whenever the meshing's convergence is questioned, the meshing can be regulated to yield convergence.

5.1.4 Conclusion

Using the setup explained in section 5.1.3, Velocity, Pressure and Vorticity Contours and the Stream line Pathlines can be obtained. As the computation is done, the Graphics section is ready for use. In the Contours section using Velocity contours, Velocity Magnitude and Vorticity Magnitude, and Pressure contour, Static pressure, and furthermore using Pathlines for Velocity, Stream Function with 50 path skips and 500 steps, the Streamline Graphics are also yielded, demonstrated in the figures later in the text, in four different methods as listed below.

It must be mentioned that the Reynolds Stress method did not converge well, as it was faced with a floating point exception error because of how small the elements were and the large Skweness number, with the original meshing so the meshing was regulated to get better results. This regulation consisted of choosing an estimated wall distance of 7.2(10⁻³); with 7 layers in the Inflation meshing and a Growth Rate of 1.1 and Maximum thickness of 0.014 m, a y+ amount of 40 is achieved (Calculated by CFD online) as it is a great amount to set the Near Wall Treatment as Scalable Wall Functions instead of Enhanced Wall Treatment! As well this Method, for the Transition (SST) Method there was also a Convergence issue which can be Resolved by using a change in the meshing and having a smaller meshing, but as a comparison between the Methods is desired, it is left unchanged in this project.

Velocity Contour regarding each method is demonstrated in the figures 5.3 to 5.6.

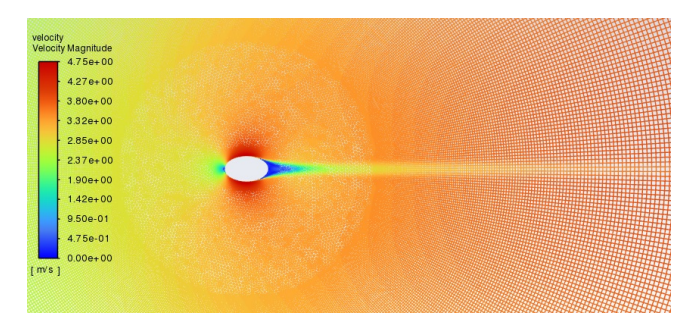


Figure 5.3: Velocity Contour for the High Reynolds, Steady, Turbulent simulation of flow against elliptical cylinder using k-epsilon (Standard) method

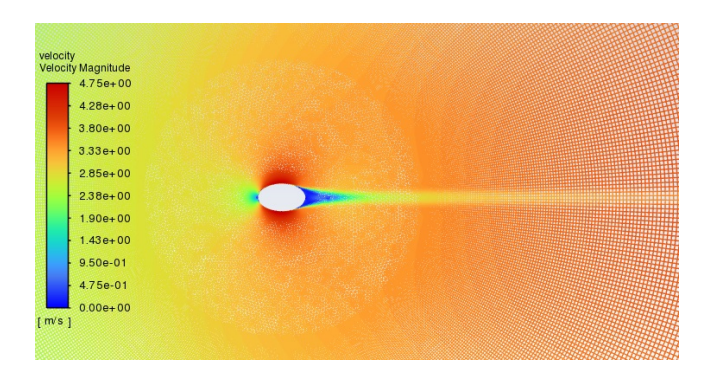


Figure 5.4: Velocity Contour for the High Reynolds, Steady, Turbulent simulation of flow against elliptical cylinder using k-epsilon (Realizable) method

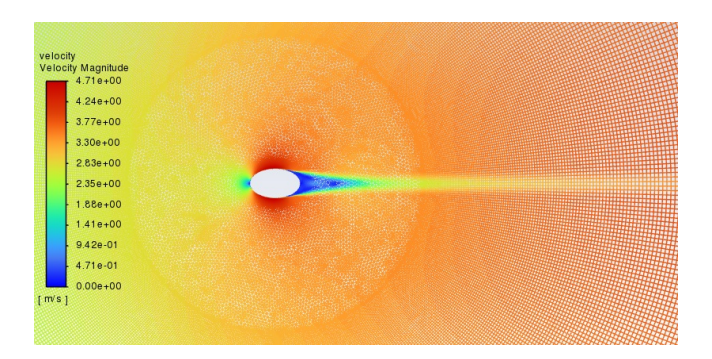


Figure 5.5: Velocity Contour for the High Reynolds, Steady, Turbulent simulation of flow against elliptical cylinder using k-omega (Standard) method

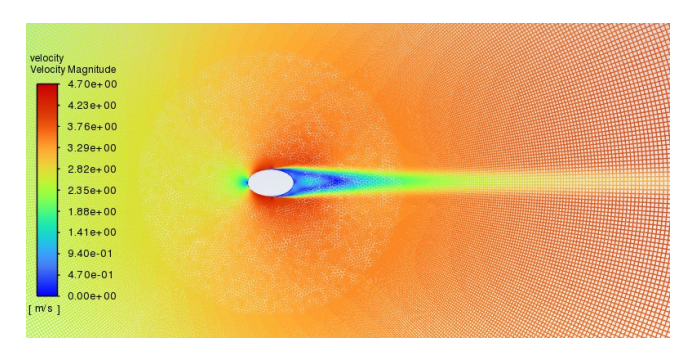


Figure 5.6: Velocity Contour for the High Reynolds, Steady, Turbulent simulation of flow against elliptical cylinder using Transition (SST) method

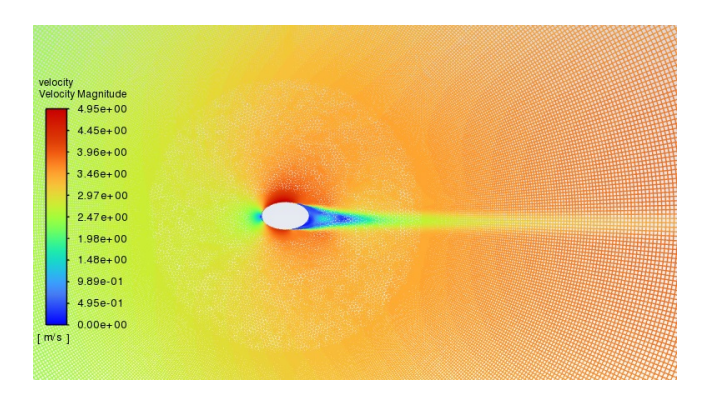


Figure 5.7: Velocity Contour for the High Reynolds, Steady, Turbulent simulation of flow against elliptical cylinder using Reynolds Stress method

Vorticity Contour regarding each method is demonstrated in the figures 5.8 to 5.12.

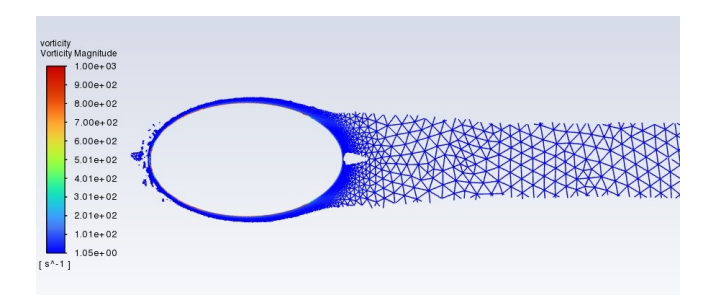


Figure 5.8: Vorticity Contour for the High Reynolds, Steady, Turbulent simulation of flow against elliptical cylinder using k-epsilon (Standard) method

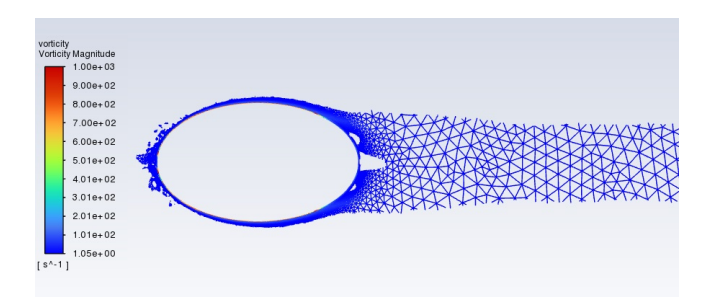


Figure 5.9: Vorticity Contour for the High Reynolds, Steady, Turbulent simulation of flow against elliptical cylinder using k-epsilon (Realizable) method

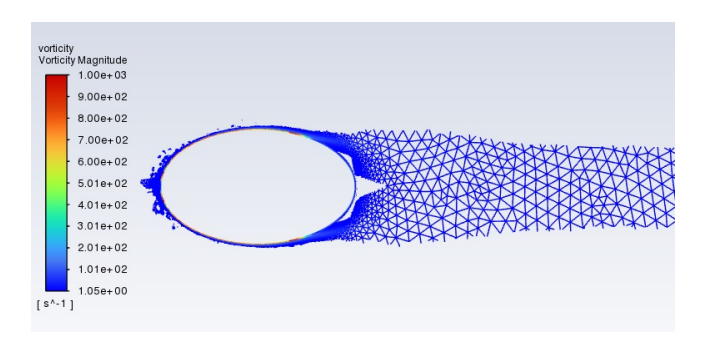


Figure 5.10: Vorticity Contour for the High Reynolds, Steady, Turbulent simulation of flow against elliptical cylinder using k-omega (Standard) method

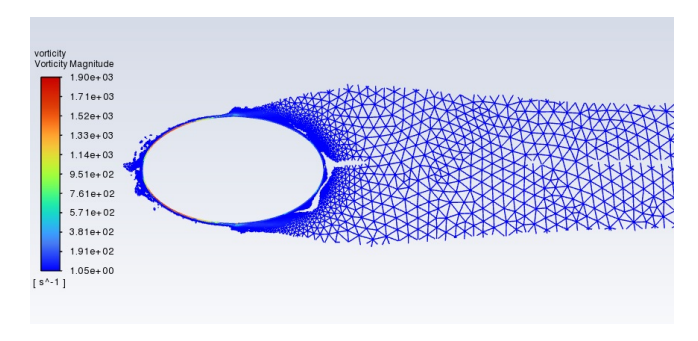


Figure 5.11: Vorticity Contour for the High Reynolds, Steady, Turbulent simulation of flow against elliptical cylinder using Transition (SST) method

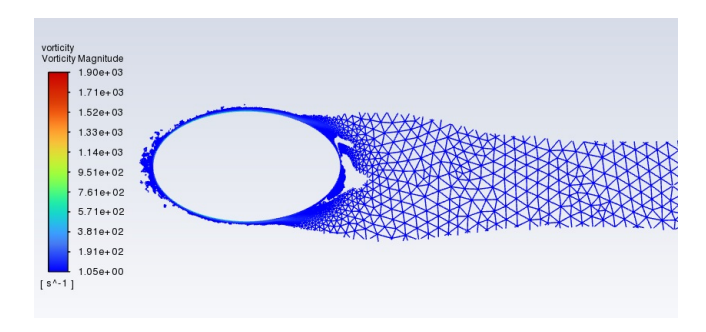


Figure 5.12: Vorticity Contour for the High Reynolds, Steady, Turbulent simulation of flow against elliptical cylinder using Reynolds Stress method

Pressure Contour regarding each method is demonstrated in the figures 5.13 to 5.17.

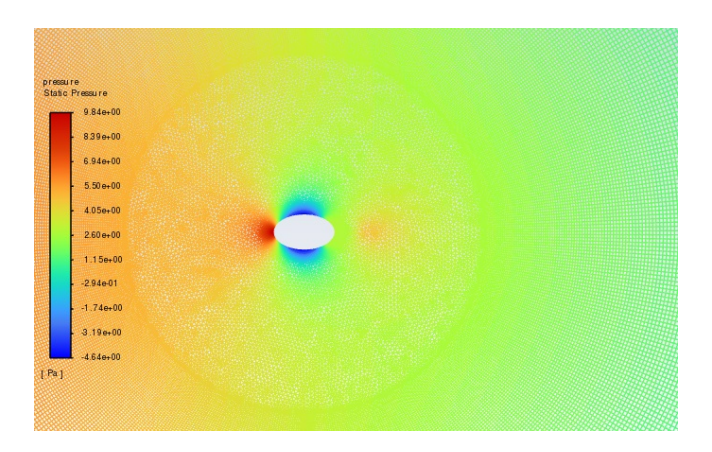


Figure 5.13: Pressure Contour for the High Reynolds, Steady, Turbulent simulation of flow against elliptical cylinder using k-epsilon (Standard) method

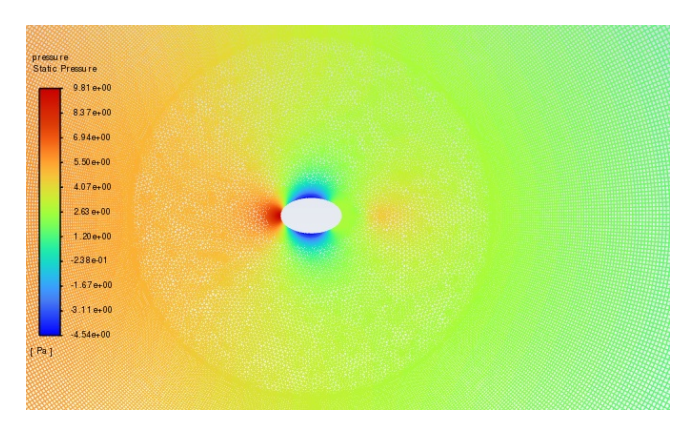


Figure 5.14: Pressure Contour for the High Reynolds, Steady, Turbulent simulation of flow against elliptical cylinder using k-epsilon (Realizable) method

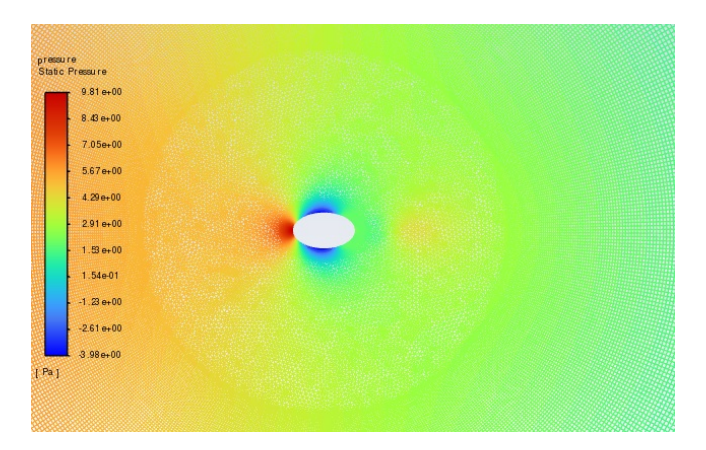


Figure 5.15: Pressure Contour for the High Reynolds, Steady, Turbulent simulation of flow against elliptical cylinder using k-omega (Standard) method

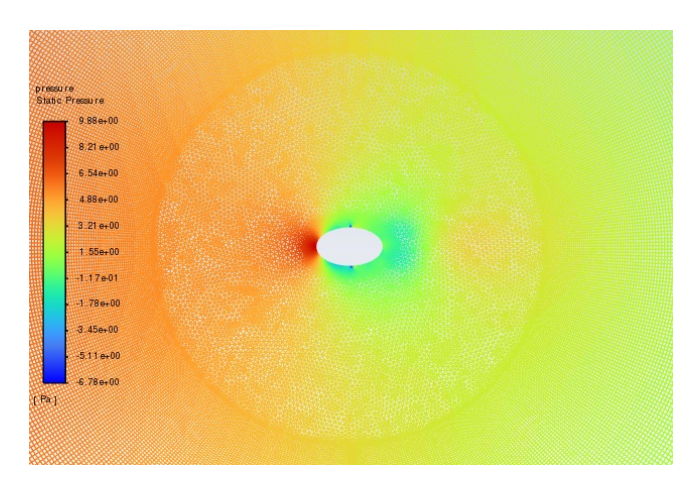


Figure 5.16: Pressure Contour for the High Reynolds, Steady, Turbulent simulation of flow against elliptical cylinder using Transition (SST) method

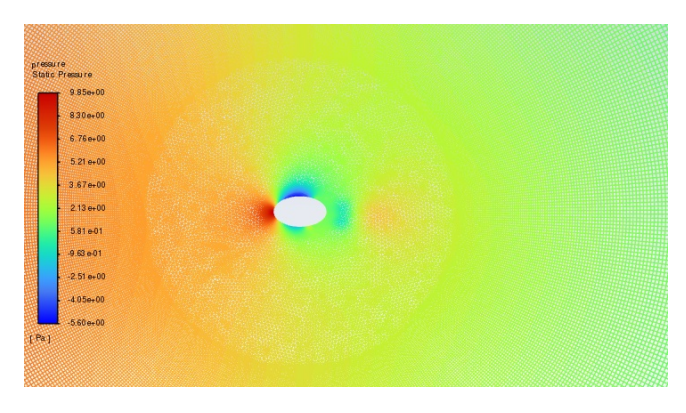


Figure 5.17: Pressure Contour for the High Reynolds, Steady, Turbulent simulation of flow against elliptical cylinder using Reynolds Stress method

Streamline Graphics regarding each method is demonstrated in the figures 5.18 to 5.22.

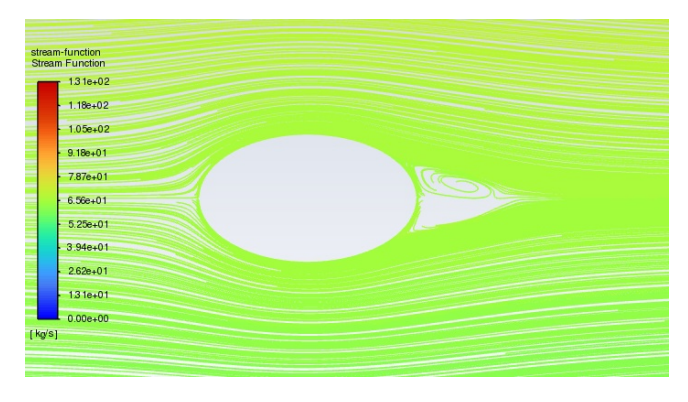


Figure 5.18: Streamline Graphics for the High Reynolds, Steady, Turbulent simulation of flow against elliptical cylinder using k-epsilon (Standard) method

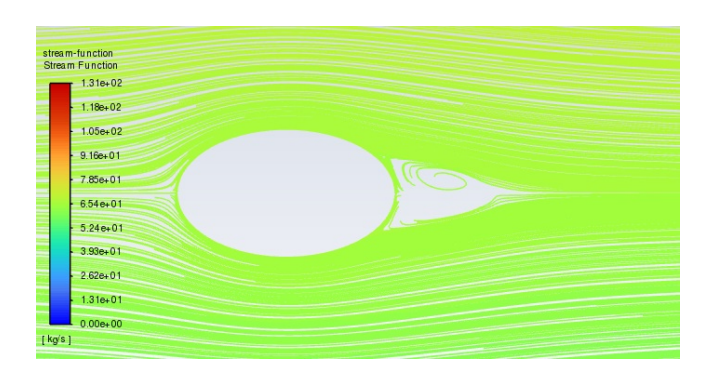


Figure 5.19: Streamline Graphics for the High Reynolds, Steady, Turbulent simulation of flow against elliptical cylinder using k-epsilon (Realizable) method

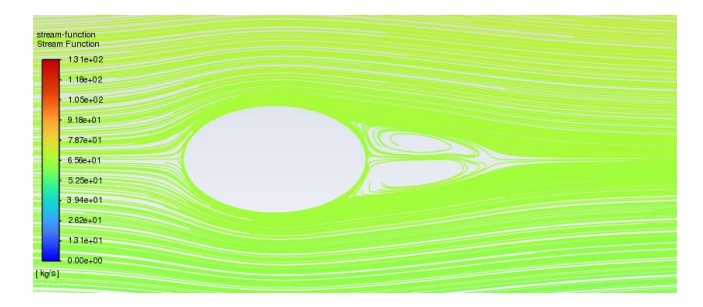


Figure 5.20: Streamline Graphics for the High Reynolds, Steady, Turbulent simulation of flow against elliptical cylinder using k-omega (Standard) method

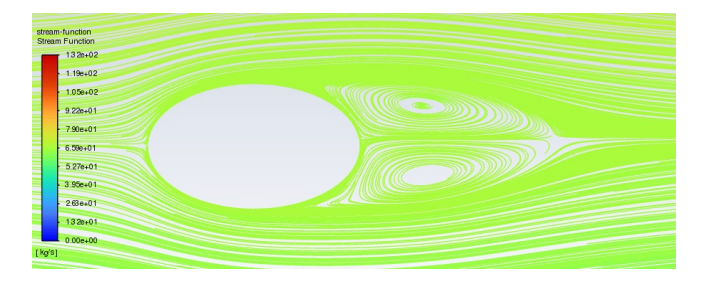


Figure 5.21: Streamline Graphics for the High Reynolds, Steady, Turbulent simulation of flow against elliptical cylinder using Transition (SST) method

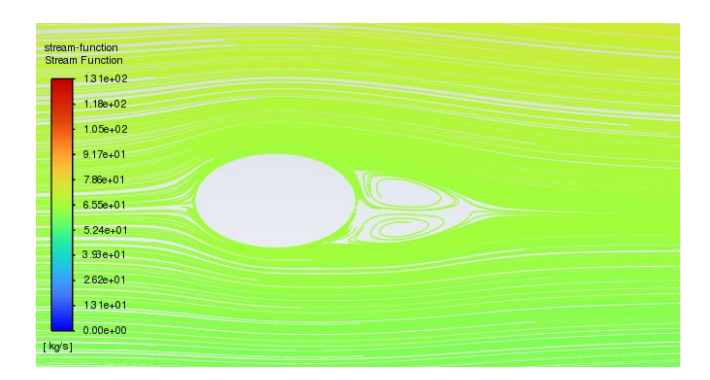


Figure 5.22: Streamline Graphics for the High Reynolds, Steady, Turbulent simulation of flow against elliptical cylinder using Reynolds Stress method

As all the Contours and Graphics explain, there is a Stagnation Point again at 0 degrees but the secondary stagnation points have moved further along the cylinder's body compared to the previous laminar flow Stagnation Points as demonstrated in the Velocity Contours, Considering the flow regime is described as Turbulent this is quite compatible with theory as the Stagnation Points must occur around 120 degrees. For the Vorticity Contours as the method used is more precise, the Stagnation Points get more and more visible as they are explicitly shown in figure 5.12, agreeing with how they happen behind the cylinder at something about 120 degrees, It is also clear how the vortices lose their kinetic energy in time and their energy becomes heat and how this lowers the Vorticity downstream.

Pressure Contours affected by the Velocity (Considering Potential Flow analysis) are precisely showing how as the flow is hit by the bluff body the pressure is at it's maximum in the Separation point at 0 degrees and how it is decreased to reach 0 at the two other Stagnation Points, Having different methods for each solution using a wide range of assumptions and equations, the Contours are ofcourse different yet they all still agree over how there are two Stagnation Points behind the body at about 120 degrees.

Method	F_D	C_D
k-epsilon (Standard)	1.5	0.19
k-epsilon (Realizable)	1.52	0.2
k-omega (Standard)	1.84	0.24
Transition (SST)	3.57	0.46
Reynolds Stress	2.3	0.3

Table 5.2: Drag Force and Drag Coefficient calculated by each Turbulence Method simulation

At last the Streamline Graphics also show remarkable grow in the length of vortices appearing behind the bluff body compared to previous Laminar Flow simulations, Showing how the Vortices are moving downstream with the flow.

A list of Drag Forces Computed by the simulation is given below and with the help of equation 5.1, from article 7.1.3 in appendix, the Drag Coefficient is Calculated.

$$C_D = \frac{F_D}{\frac{1}{2}\rho V^2 A_L}, A_L being the Body Lateral Projected Area Parallel To Flow$$
 (5.1)

As it is also analyzed in the article (Table 10), the Drag Coefficient in experimental conditions is about 0.6, the most precise simulation must be that of Transition (SST) and Reynolds Stress method which have about 25% to 50% variance with this amount. Considering this is a very rough estimation and not a perfect simulation rather a preliminary one, the variance is well acceptable.

6. Concluding remarks

Altogether the different configurations can be compared to each other yielding a chart like below.

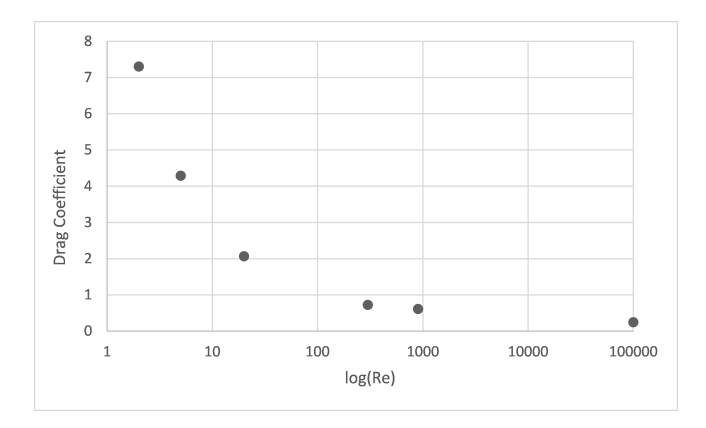


Figure 6.1: Simulation's computed Drag Coefficient in different Reynolds Configurations as in Table 2.1

Regarding this chart, it is obvious how it is close to the results obtained for a Circular Cylinder, discussed in the book shared in appendix 7.2 (Figure 9.21). As the Elliptical Surface in question is a more streamlined body than a Circular one, therefore it's Drag Coefficient is also less than the one for Circular Cylinder explained above (and the data for the Circular Cylinder is very close to what it has to be based on the figure shared in the book). A summary of the Streamline Graphics is demonstrated below.

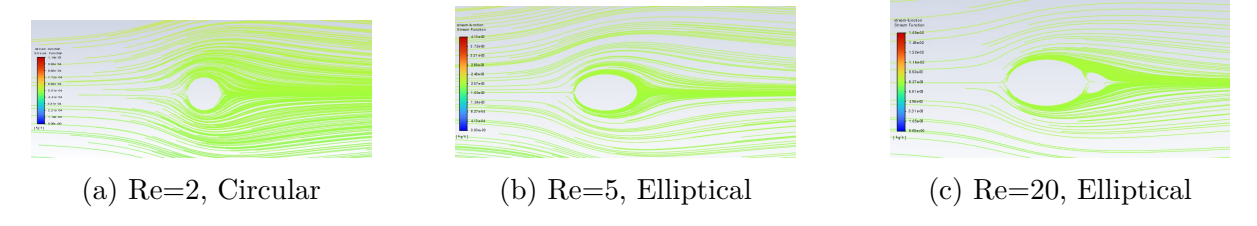


Figure 6.2: Streamline Graphics for Steady Laminar Flows

^{*}The simulation's result for Turbulent Configuration is placed as an average.

^{**} The first data in the Chart is related to a Circular Surface and the rest are of an Elliptical Cylinder

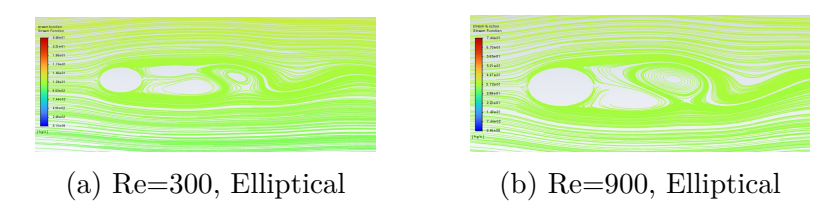


Figure 6.3: Streamline Graphics for Transient Laminar Flows

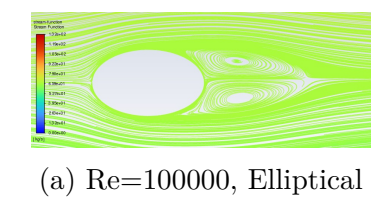


Figure 6.4: Streamline Graphics for Steady Turbulent Flows

Regarding the results obtained by the Simulation, are in accordance with the figure shared in article 7.3.5, regarding Elliptical Cylinders in moderate Reynolds regimes. As expected at first the flow passes the body without any Separation occurring considering the low Reynolds number, further on as the Reynolds number is increased a little there are Vortices created behind the bluff body which are symmetrical and attached to the body and not moving downstream, after increasing the Reynolds number even more, larger vortices are reached yet they are still not moving downstream. As the Flow Reynolds is getting closer to it's Critical value, the flow becomes unsteady, transitioning from laminar to turbulent, in these configurations, the flow has become naturally unsteady, resulting in unsteady movement of bigger eddies and smaller ones up and down as is clear in the graphs and also in the animations of appendix 7.4, In these Laminar yet Transient cases, as was explained before the Stagnation points occur closer to the left side of the cylinder, on the other hand as there is a Steady Turbulent flow, these Stagnation points are moved forward to a position on the right side of the cylinder. This change in the position of the Stagnation points is of importance and is due to the flow's momentum, as laminar flow has less momentum regarding it's smaller eddies and it's combination of microscopic and macroscopic momentum exchange, it's Separation Points occur rather sooner and on the left side of the Cylinder, for Turbulent flow, this is not accurate since it's momentum exchange is ruled by it's bigger eddies and total macroscopic momentum exchange is occurring, therefore it has a larger momentum and has more power facing the adverse pressure gradient, resulting in it's stagnation points falling on the right side of the Cylinder!

As the eddies movements are more visible perhaps in the animations of appendix 7.4, their larger vortices and obvious movement downstream leads us to the understanding that they are just the Von Kármán vortex street we have been looking for!

7. Appendix

7.1 Articles

7.1.1 Fluid Flow Around and Heat Transfer from Elliptical Cylinders, 2005

https://drive.google.com/file/d/1MZKqKVUrjG7haU4xo3IbQsiT9ZnplxOK/view?usp=drive_link

7.1.2 Steady flow of power-law fluids across an unconfined elliptical cylinder, 2006

https://drive.google.com/file/d/1IZAaklb17EukUjuO1vJxzM1Bl1tTYPSn/view?usp=drive_link

7.1.3 Summary of drag coefficients of various shaped cylinders, 1957

https://drive.google.com/file/d/1NG5aDshQn5yVHmpX1HWUZGkfQlza-Z4e/view?usp=drive_link

7.1.4 Vortex dynamics in the wake, 1996

https://drive.google.com/file/d/1ATOX4yAS4qGJM6WplN8mANrmIFGJFZ0i/view?usp=drive_link

7.2 Books

7.2.1 Fundamentals of Fluid Mechanics, Edition six

https://drive.google.com/file/d/14ZwBUjFiD5qdRwUictpCgWnEoAjn3Ls5/view?usp=drive_link

7.3 Additional articles

7.3.1 Vorticity diffusion and boundary layer

https://drive.google.com/file/d/15n86Nj8Q7NuOVDTc1BHdCX8XWaX86ZK-/view?usp=drive_link

7.3.2 Boundary layers

https://drive.google.com/file/d/10oVtZD4ZqKisvgsyEgayviWhIOm_N6xH/view?usp=drive_link

7.3.3 A review of experiments on stationary bluff-body wakes

https://drive.google.com/file/d/10GfM7iC1BQ6QgUzdI5n8QS8Rvv7mv3Ng/view?usp=drive_link

7.3.4 From the circular cylinder to the flat plate wake: The variation of Strouhal number with Reynolds number for elliptical cylinders

https://drive.google.com/file/d/1y3rhbUkXxLHXx2RA2bgsEKN8DQjc7QMM/view?usp=drive_link

7.3.5 Flow around elliptical cylinders in moderate Reynolds numbers

https://drive.google.com/file/d/1GIK28A33xouEZrAitt5TvDbLEuowP2CJ/view?usp=drive_link

7.3.6 Strouhal determination for several regular polygon cylinders

https://drive.google.com/file/d/1Lh6aIKESfOP_OYIvenrergRTqfmsAOPD/view?usp=drive_link

7.3.7 Direct Numerical Simulation of Flow Past Elliptic Cylinders

https://drive.google.com/file/d/1upk2eE1abCsWlVHN-lb1ddhw7yWzoYB_/view?usp=drive_link

7.4 Animations

7.4.1 Velocity animation for the Transient, Laminar regime in Moderate Reynolds

This animation has been obtained from the Results section, and the frames were saved every 5 Time Steps. https://drive.google.com/file/d/1DjpSssfOnL45rDCVtxyM3x7XrC5aPDys/view?usp=drive_link

7.4.2 Velocity animation for the Transient, Laminar regime in High Reynolds

This animation has been obtained from the Results section, and the frames were saved every 5 Time Steps. https://drive.google.com/file/d/1vMaywEJ6aWyndKWwL6RTJqgLs_kX0gxV/view?usp=drive_link